

Figure 3. WT ATRIP cDNA but not cDNA encoding p.Arg760* ATRIP complements the G2/M checkpoint defect in CV1720 cells, and p.Arg760*ATRIP impairs ATR-ATRIP protein interaction. A) Analysis of the G2/M checkpoint defect in CV1720 cells following expression of ATRIP cDNA. G2/M checkpoint arrest was examined 2 h post exposure to 5 J m^{-2} UV. As shown in Figure 1A, WT cells showed proficient checkpoint arrest whilst DK0064 (ATR-SS) and CV1720 (patient) cells are unable to undergo arrest. Expression of WT ATRIP cDNA restored the ability of CV1720 (patient) and DK0064 (ATR-SS) to undergo checkpoint arrest but this was not observed following transfection of cDNA encoding R760* ATRIP. Significantly, expression of ATRIP R760* did not impair checkpoint arrest in WT cells verifying that it does not exert a dominant negative impact. Results represent the mean and SD of three experiments. WT cells were GM2188. ATR-SS represents DK0064 and patient, CV1720. B) R760* ATRIP impairs ATR-ATRIP interaction. Crude lysates were prepared from HEK293T cells and either mock transfected (lane1), transfected with HA-tagged WT ATRIP cDNA (lane2), or R760* ATRIP cDNA (lane3) (generating p.Arg760* ATRIP protein) together with ATR cDNA. The extracts were immunoprecipitated with agarose-conjugated rabbit anti-HA-tag antibody (MBL). Interaction with ATR was examined by immunoblotting with ATR antibodies (left panel). Immunoblotting using the HA-tag (ATRIP; right panel) verified expression of the appropriately sized ATRIP in the samples. 33% of the crude lysate was loaded; IP, immunoprecipitate.
doi:10.1371/journal.pgen.1002945.g003

(ATR-SS) cells (Figure 5A) [7]. Checkpoint arrest after exposure to ionising radiation was activated normally. Additionally, we examined the phosphorylation of a range of ATR substrates following exposure to 0.5 mM HU and observed impaired phosphorylation in both 27-4BI and 19-8BI cells (Figure 5B). Collectively, these functional data substantiate a deficiency in the ATR-dependent DNA damage response in LBLs from these two cases. Thus, we conclude that both patients represent further ATR-SS patients.

Discussion

Although the first causal defect for SS was identified as ATR in 2003, further patients with mutations in ATR have not been reported [7]. SS patients are characterised by microcephaly and growth delay, features also observed in other microcephalic, primordial dwarfism syndromes including MOPD type II and MGS. Given that all ATR-SS patients to date share consanguinity, there are limitations in defining the spectrum of clinical features conferred by ATR deficiency to support a clinical distinction between ATR-SS and related disorders such as MOPD type II and MGS as well as other sub-classes of SS [1–3,31].

Here, we describe the novel identification of a patient mutated in ATRIP, the binding partner of ATR. Thus, we identify ATRIP

as a new causal gene for SS. The mutational change in one ATRIP allele lies within a region previously suggested to be required for interaction with ATR, which is consolidated by our work [21,30]. We demonstrate that the second allele is abnormally spliced causing a reduction in ATRIP mRNA from that allele. qRT-PCR analysis suggested that there could be 25% residual WT ATRIP expressed in the patient cells. Consistent with this, we routinely observed ~10–20% of WT ATRIP protein in CV1720 cells by Western Blotting, although the level was variable between preparations. Although not examined in detail, there appeared to be a correlation between proliferation status and ATRIP levels, with the levels decreasing as proliferation slowed. Thus, differences in the proliferative state of cells at the time of analysis may underlie the apparent difference between Western Blotting and qRT-PCR analysis. Notwithstanding some limitations in quantification, the patient clinical features were marked despite ~10–20% residual ATRIP expression. Similarly, in patient DK0064, residual ATR protein can be readily detected [7]. Thus, we conclude that reduced but detectable levels of ATR/ATRIP protein can confer a clinical phenotype.

Additionally, we identify two further SS patients with ATR mutations in two unrelated families native to the UK. Interestingly, despite being unrelated, 27-4BI and 19-8BI carry the same compound heterozygous mutations, possibly representing founder mutations in the UK population.

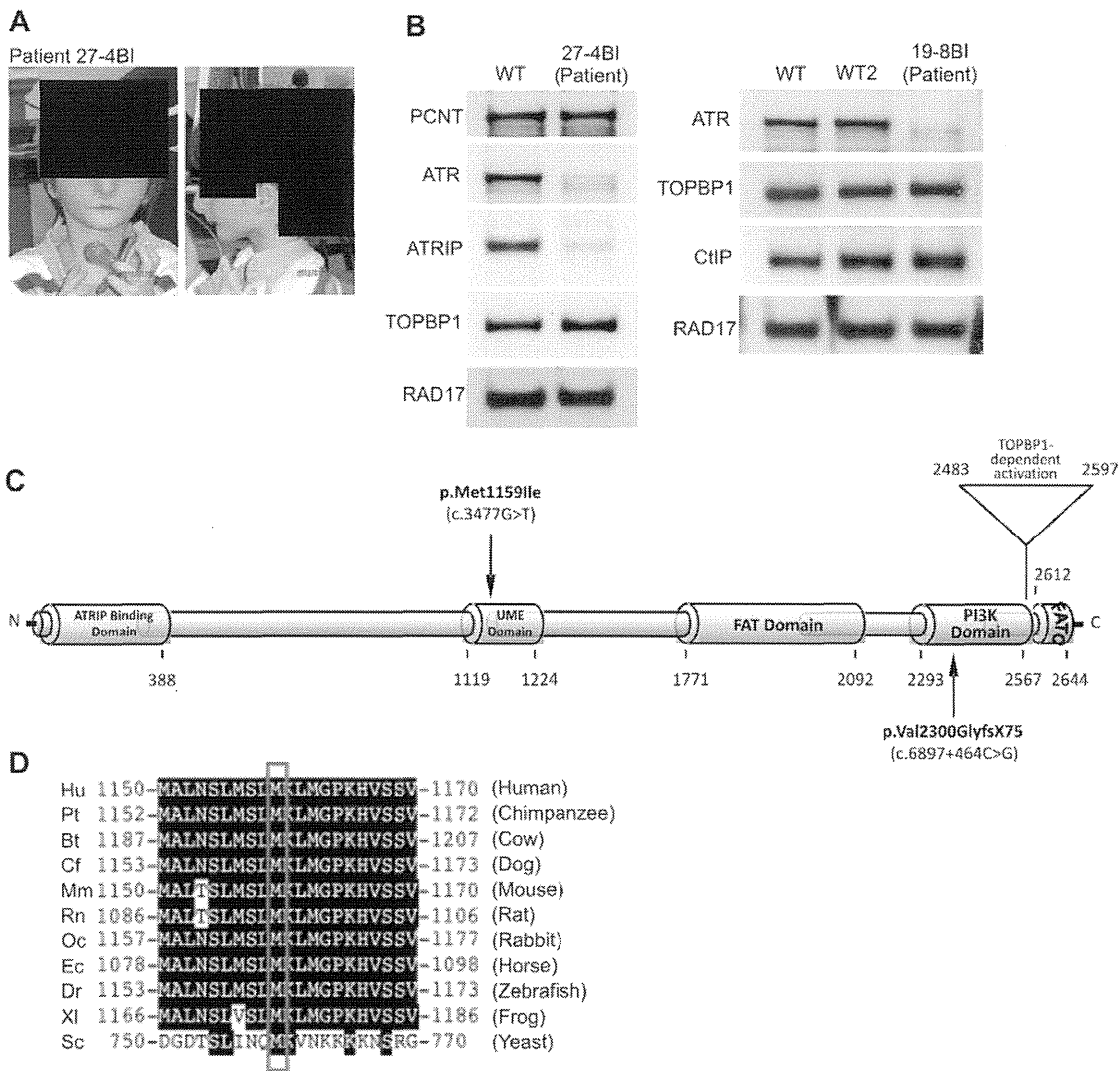


Figure 4. Patients 27-4BI and 19-8BI have reduced ATR and ATRIP expression and mutations in ATR. A) Photographs of patient included with informed consent of parent. B) Cell extracts (50 μ g) from LBLs derived from WT (IM257), patient 27-4BI or patient 19-8BI were immunoblotted using the indicated antibodies. Reduced expression of ATR was observed in both patients. 27-4BI also had reduced ATRIP expression. C) Structure of ATR showing the site of the mutations identified and the UME domain. D) The UME domain is conserved between species and the methionine residue within this domain is conserved in yeast. doi:10.1371/journal.pgen.1002945.g004

All four ATR/ATRIP patients displayed severe microcephaly and growth delay (Table 1). All patients also displayed micrognathia, receding forehead, dental crowding and microtia with small or absent lobes (Figure 4A). Interestingly, an MRI scan of the ATRIP-SS patient revealed an abnormally small pituitary with absent fossa, which could contribute to the delayed growth observed (Figure S1). In distinction to the original ATR-SS patient (DK0064), patients 27-4BI and 19-8BI showed more marked skeletal abnormalities including digital features and aberrant patellae suggesting that ATR deficiency can have a detrimental impact on bone development (Table 1, Figure S4) [32]. Interestingly, aberrant patellae is a clinical feature commonly exhibited by MGS patients suggestive of a biological overlap between the ATR checkpoint pathway and the replication

machinery during skeletal development and maintenance. In keeping with this, characterisation of a mouse model harbouring the same mutational change identified in the original ATR-SS patient (DK0064) revealed marked bone abnormalities including kyphosis and osteoporosis [32]. Our findings suggest that ATR-ATRIP SS shows more overlap with MGS than previously recognised (Table 2). However, whereas ATR-ATRIP SS patients tend to have very marked microcephaly, growth delay, dental crowding, small ears and less severe skeletal abnormalities, the spectrum for MGS tends to be less marked microcephaly and growth delay but a striking impact on skeletal development. Nonetheless, there does not appear to be an absolute clinical divide between these two disorders. Significantly, these overlapping clinical features could reflect the fact that both ATR/ATRIP

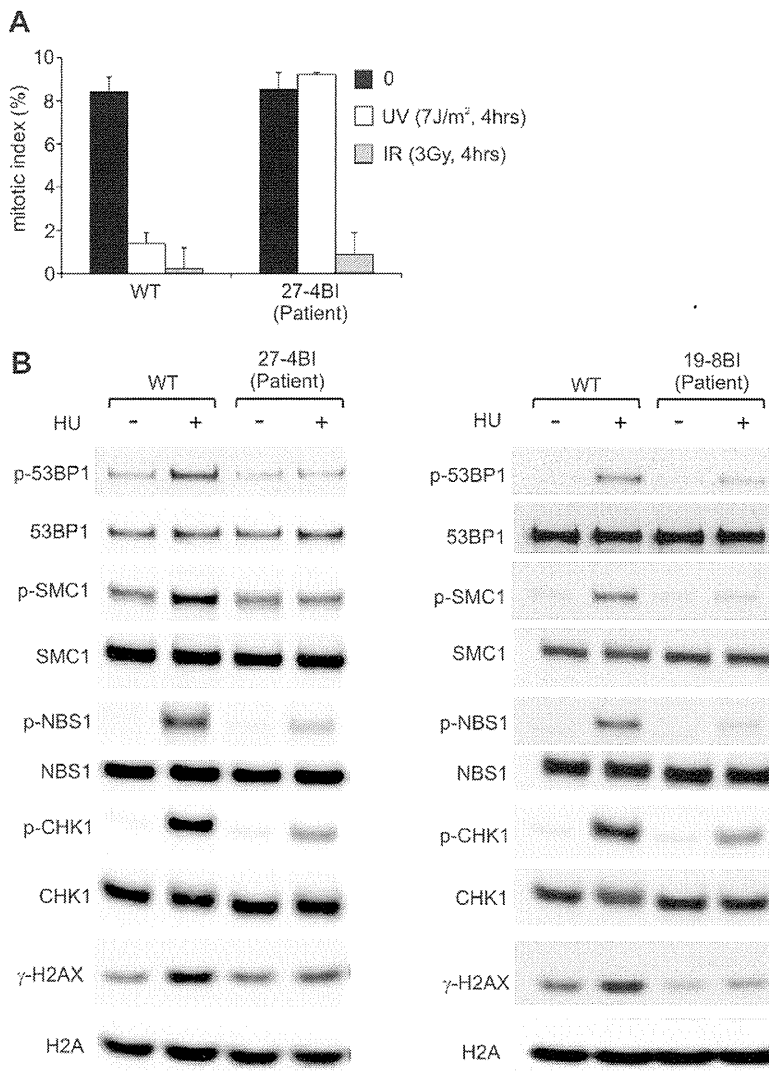


Figure 5. LBLs from patient 27-4BI and 19-8BI showed impaired ATR-dependent damage responses. A) 27-4BI cells were examined for their ability to activate G2/M checkpoint arrest at 4 h following exposure to 7 J m^{-2} UV. In contrast to WT cells (GM2188), no significant arrest was observed in 27-4BI cells. The checkpoint response to ionizing radiation, which is ATM rather than ATR dependent, was normal. B) LBLs derived from patients 27-4BI and 19-8BI were examined for their ability to phosphorylate the indicated ATR substrates at 1 h following exposure to 0.5 mM HU. WT represents IM257. 27-4BI and control LBLs have a similar cell cycle profile demonstrating that the lack of ATR substrate phosphorylation cannot be attributed to the lack of S phase cells (Figure S2).
doi:10.1371/journal.pgen.1002945.g005

and the origin licensing complex play an essential role in promoting efficient replication and recovery from fork stalling, which may be vital during developmental stages involving rapid replication [13].

In summary, we provide the first report of a SS patient with mutations in *ATRIP*, defining a further novel genetic defect for this disorder, and describe two additional patients native to the UK, with mutations in *ATR*. The description of multiple ATR-ATRIP patients allows us to define a spectrum of clinical features conferred by *ATR-ATRIP* mutations. The clinical characteristics include severe microcephaly and growth delay, small or absent ear lobes, micrognathia and dental crowding. In addition, the novel ATR-mutated cases described here expand the clinical impact of impaired ATR-function to include more marked skeletal involvement.

Methods

Ethics Statement

Ethical approval for the research was granted by the School of Life Sciences Research Governance Committee, University of Sussex. Informed consent was obtained and clinical investigations were conducted according to the principles expressed in the Declaration of Helsinki. Patient material was gathered under conditions of the Human Tissue Authority (HTA licence number 12119).

Patients and cell lines

CV1720 is a SS patient of Gujarati-Indian origin. Patients 27-4BI and 19-8BI are English. The clinical features are described in

Table 2. MGS and Seckel syndrome patient phenotypes.

	ORC1 - MGS	Pre-RC MGS	ATR/ATRIP SS
Number of patients	10	25	4
OFC (cm)*	-5.4 to -11 SD	+1.7 to -5.0 SD	-10 to -12 SD
Height (cm)*	-4.5 to -9.6 SD	-0.4 to -6.4 SD	-5 to -8 SD
Weight (kg)*	0.8 to -11 SD	-0.3 to -9.9 SD	-3.3 to -8 SD
Intellectual disability	Ranges from none to mild/moderate	None	Developmental delay (2/4)
Facial Features	Small and abnormal ears (9/10), micrognathia (5/10), down slanted palpebral fissures (1/10)	Small and abnormal ears(25/25), micrognathia (20/25), down slanted palpebral fissures (8/25)	Small and/or abnormal ears (4/4), micrognathia (4/4), receding forehead (4/4), prominent nose (4/4), short palpebral fissures (2/4)
Skeletal abnormalities	Delayed bone age (3/10), Slender long bones (2/10) , absent patellae (6/10), genu recurvatum (4/10)	Delayed bone age (11/25), slender long bones, absent patellae (24/25)	Delayed bone age (1/4), 5 th finger clinodactyly (2/4), symmetric dwarfism (3/4), small/abnormal patellae (2/4), kyphosis (1/4), hip abnormality (2/4), narrow pelvis (iliac blades) (1/4)
MRI	Normal in 2 patients examined	NA	Generalised cerebral atrophy, delayed myelination, abnormal gyration (2 patients examined)
Other	High pitched voice (1/10), full lips (7/10), cryptochordism (2/4 examined), mammary hypoplasia (2/2 examined), feeding and respiratory problems during infancy (8/10)	Full lips (14/25), cryptochordism (7/14 examined), mammary hypoplasia (8/8 examined), feeding (20/25) and respiratory (9/25) problems during infancy	Dental crowding (4/4), feeding and respiratory problems during infancy (1/4)

*standard deviations from the age-related normal population mean, NA = not assessed. MGS data from [13,14] [33,34]. doi:10.1371/journal.pgen.1002945.t002

Table 1. Lymphoblastoid cell lines (LBLs) were derived from blood following EBV transformation. WT LBLs were GM2188 or LB197 as indicated. All LBLs were grown in RPMI medium supplemented with 10% foetal calf serum, penicillin, and streptomycin. Transfection with *ATRIP* cDNA was with Genejuice Transfection Reagent (Novagen, Merck Millipore, UK) following the manufacturers protocol.

qRT-PCR. Transcript levels of the *ATRIP*-c.2278C (normal) and *ATRIP*-c.2278C>T (p.Arg760*) alleles in LBLs from patient CV1720, and the parents were determined by the cycleave quantitative real time PCR (Cycleave-qPCR, TaKaRa Co. Ltd, Kyoto Japan) as well as standard site specific q-PCR (carried out in triplicate). Transcripts from the *HPRT1* allele were used as a quantification control. In the Cycleave qPCR, RNaseH sensitive fluorescent probes that specifically recognize the c.2278C and c.2278C>T alleles were used for the assay. qPCR results were analyzed by the $\Delta\Delta CT$ method. qPCR primers and probes used for the assay are listed below. (172F, 5'-CTTCACTGCCGAC-GACCTGG-3'; 191R, 5'-TTTGCTCGTTCCTGCTG-3'; P1, 5'-GGGGTCAGCATGCTCATCC-3'; P2, 5'-GGGGGTC-AGCATGCTCATCT-3'; P3C, 5'-ACCTCGGGGTCTTCCA-CATC-3'; P4, 5'- -3'; P5, 5'- -3'; P6C, 5'- -3'; P7, 5'-GCC-TATCGCAGAAGGACAAG-3'; P8, 5'-GGGTCTTCCACAT-CGGTTTC-3'; probe1 for c.2278C, 5'Eclipse-CCCTC(rG)GAT-3'FAM; probe2 for c.2278C, 5'Eclipse- GCCCTC(rA)GA-3'ROX)

Co-immunoprecipitation. To investigate the interaction of the ATRIP proteins with ATR, HEK293T cells were transfected with the HA-tagged *ATRIP* cDNA expressing plasmids (wild type and 2278C>T *ATRIP*) together with *ATR* cDNA, followed by 24 h incubation. Whole cell lysates were prepared using CelLytic Nuclear Extraction Kit (Sigma, St. Louis). Co-immunoprecipitation was performed using rabbit anti-HA antibody-conjugated agarose beads (MBL, Nagoya, Japan). Western blotting was carried out using ATR or anti-HA (detecting HA-tagged ATRIP) antibodies. Anti-ATR was N19 (Santa Cruz, Santa Cruz) at 1:200

dilution. Anti-HA-tag antibody, 132-3 (MBL, Nagoya, Japan), was used at 1:1000 dilution.

Immunofluorescence for analysis of γ H2AX and 53BP1 staining

Cells were cytospun onto slides, fixed with 3% formaldehyde for 10 min and permeabilized in 0.5% Triton-X100. After antibody treatment and staining with 4,6-diamidino-2-phenylindole (DAPI), coverslips were mounted in Vectashield mounting medium (Vector Laboratories, Burlingame). Samples were incubated with primary antibodies for γ -H2AX (Millipore, Billerica) or 53BP1 (Bethyl, Montgomery). Secondary antibodies were from Sigma (St. Louis).

Western blotting

Cells were lysed for one hour in IPLB (50 mM Tris-HCl, 150 mM NaCl, 2 mM EDTA, 2 mM EGTA, 25 mM NaF, 25 mM β -glycerolphosphate, 0.1 mM NaOrthovanadate, 0.2% Triton X-100, 0.3% NP-40, plus protease inhibitor cocktail (Roche, Basel) at 4°C, centrifuged at 13,000 rpm for 10 minutes. The soluble fraction was subjected to SDS-PAGE and transferred to a nitrocellulose membrane for protein detection.

Antibodies raised against ATR, CHK1 (FL476) and MCM2 (N19) were from Santa Cruz (Santa Cruz). Anti-FANCD2, ATRIP and phospho-Chk1 (Ser317) antibodies were from Novus (Littleton), Bethyl (Montgomery), and Cell Signaling (Beverly, Woburn), respectively.

G2/M checkpoint arrest

Cells were exposed to 5 or 7 Jm⁻² UV, or 3Gy ionising radiation and incubated for 2 or 4 hours (as indicated) in complete medium containing 0.2 ug/ml Colcemid (Invitrogen, Carlsbad), followed by processing for immunofluorescence as detailed above. Mitotic cells were detected by α -Histone H3-pSer10 antibodies (Millipore, Billerica) and cells were counterstained with DAPI.

Supporting Information

Figure S1 Photograph of limbs and MRI scan of patient CV1720. Left hand photograph showing hands and feet. Right hand photograph shows an MRI scan where a small pituitary is evident. (TIF)

Figure S2 Cell cycle analysis of WT, DK0064 (ATR-SS), 27-4BI, and CV1720 patient LBLs. A) Asynchronous growing cultures of WT, DK0064 (ATR-SS), 27-4BI and CV1720 patient cells were pelleted, fixed in 70% ice-cold ethanol and stained with propidium iodide prior to FACs analysis. Populations were gated and the proportion of cells in G1, S and G2/M phases of the cell cycle measured. B) WT, DK0064 (ATR-SS), 27-4BI and CV1720 patient cells were treated with nocodazole for 16 h and then fixed and analysed as in a). C) Asynchronous growing cultures of WT, DK0064 (ATR-SS), 27-4BI and CV1720 patient cells were pulse-labelled with 50 μ M BrdU for 1 h. Cells were then fixed in 70% ice-cold ethanol and processed for BrdU FACs analysis as described in Bicknell et al, 2011 [13]. The proportion of cells in S phase were gated and measured. Each graph represents the mean of three independent experiments. The error bars represent the standard deviation. (TIF)

Figure S3 Identification of a truncating mutation in *ATRIP* in patient, CV1720. Genomic DNA sequencing of *ATRIP* exons showed that patient CV1720 and the unaffected mother, CV1780, are heterozygous for a c.2278C>T mutational change in exon12 of *ATRIP*. The father has a WT sequence at this site. 2278C>T generates a primary stop codon predicting a truncated protein at position arginine 760 (p.R760*). WT sequence shown in blue, the mutation is shown in Red. (TIF)

Figure S4 Photographs of patients 27-4BI and 19-8BI. A) Shows abnormal digits of patient 27-4BI. B) Copper beaten appearance of skull of patient 19-8BI. C) Frontal and Lateral view of left knee of patient 19-8BI showing an absence of ossification of the patella. (TIF)

Figure S5 Mutational changes observed in *ATR* in patients 27-4BI and 19-8BI. A) c.3477G>T mutational change in patients 27-4BI and 19-8BI. RT-PCR sequencing revealed a heterozygous 3477G>T mutational change in both patients causing an amino

acid substitution, p.Met1159Ile, which lies within a conserved UME (NUC010) domain of ATR. B) A double sequence was observed at the boundary between exons 40 and 41 in both patients. Sequencing showed that the double sequence was caused by insertion of a 142 bp region from intron 40. C) A C to G mutational change was observed in intron 41 of both patients converting the sequence CAGCT to CAGGT, a splice site. The insertion causes a frameshift and a stop codon at p.Val2300-Glyfs*75. D) Diagram showing the likely origin of the insertion observed at the exon 40/41 boundary. Sequencing of intron 40 revealed a C>G mutation as indicated creating a cryptic splice site causing splicing of exon 40 to the indicated intronic sequence (which represents an Alu repeat sequence). Thus one ATR allele of the patients harbours a 142 nucleotide insertion between exons 40 and 41. Exons 40 and 41 are highlighted in green and the inserted intronic sequence is shown in red. The intronic C>G change is highlighted in red. The insertion causes a frameshift and a stop codon at c.6978 in exon 41. (TIF)

Table S1 The table shows the position of single nucleotide polymorphisms identified in intron 1 and 2 in the patient and parental genomic DNA. * The contig position is defined as the position of the single nucleotide variant (SNV) on the contig (NT_022517.17) when counting from the first base (base position = 1). **rs# is the NCBI's reference SNP ID. *** minor allele (indicated as a base) and its frequency (MAF) (second most frequent allele) in a default global population reported in dbSNP database (1000 Genome phase 1, May 2011). N.A. not available. (DOCX)

Acknowledgments

We thank Dr. E. Riballo and P. Gajwani for contributions to this work and Dr. D. Cortez for providing *ATRIP* cDNA.

Author Contributions

Conceived and designed the experiments: TO GSS AMRT MO PAJ. Performed the experiments: SW TS SL GC MM NM YN. Analyzed the data: TO TS GSS AMRT MO PAJ. Contributed reagents/materials/analysis tools: EH KP MS PJB PV MB. Wrote the paper: PAJ. Aided in writing the paper: MO GSS TO AMRT.

References

- Majewski F, Goecke T (1982) Studies of microcephalic primordial dwarfism I: approach to a delineation of the Seckel syndrome. *Am J Med Genet* 12: 7–21.
- Hall JG, Flora C, Scott CI, Jr., Pauli RM, Tanaka KI (2004) Majewski osteodysplastic primordial dwarfism type II (MOPD II): natural history and clinical findings. *Am J Med Genet A* 130: 55–72.
- Gorlin RJ (1992) Microtia, absent patellae, short stature, micrognathia syndrome. *J Med Genet* 29: 516–517.
- Thornton GK, Woods CG (2009) Primary microcephaly: do all roads lead to Rome? *Trends Genet* 25: 501–510.
- Goodship J, Gill H, Carter J, Jackson A, Splitt M, et al. (2000) Autozygosity mapping of a seckel syndrome locus to chromosome 3q22.1-q24. *Am J Hum Genet* 67: 498–503.
- Borglum AD, Balslev T, Haagerup A, Birkebaek N, Binderup H, et al. (2001) A new locus for Seckel syndrome on chromosome 18p11.31-q11.2. *Eur J Hum Genet* 9: 753–757.
- O'Driscoll M, Ruiz-Perez VL, Woods CG, Jeggo PA, Goodship JA (2003) A splicing mutation affecting expression of ataxia-telangiectasia and Rad3-related protein (ATR) results in Seckel syndrome. *Nature Genetics* 33: 497–501.
- Qvist P, Huertas P, Jimeno S, Nyegaard M, Hassan MJ, et al. (2011) CtIP Mutations Cause Seckel and Jawad Syndromes. *PLoS Genet* 7: e1002310. doi:10.1371/journal.pgen.1002310
- Al-Dosari MS, Shaheen R, Colak D, Alkuraya FS (2010) Novel CENPJ mutation causes Seckel syndrome. *J Med Genet* 47: 411–414.
- Kalay E, Yigit G, Aslan Y, Brown KE, Pohl E, et al. (2011) CEP152 is a genome maintenance protein disrupted in Seckel syndrome. *Nat Genet* 43: 23–26.
- Griffith E, Walker S, Martin CA, Vagnarelli P, Stiff T, et al. (2008) Mutations in pericentrin cause Seckel syndrome with defective ATR-dependent DNA damage signaling. *Nat Genet* 40: 232–236.
- Rauch A, Thiel CT, Schindler D, Wick U, Crow YJ, et al. (2008) Mutations in the pericentrin (PCNT) gene cause primordial dwarfism. *Science* 319: 816–819.
- Bicknell LS, Walker S, Klingseisen A, Stiff T, Leitch A, et al. (2011) Mutations in ORC1, encoding the largest subunit of the origin recognition complex, cause microcephalic primordial dwarfism resembling Meier-Gorlin syndrome. *Nat Genet* 43: 350–355.
- Bicknell LS, Bongers EM, Leitch A, Brown S, Schoots J, et al. (2011) Mutations in the pre-replication complex cause Meier-Gorlin syndrome. *Nat Genet* 43: 356–359.
- Willems M, Genevieve D, Borck G, Baumann C, Baujat G, et al. (2010) Molecular analysis of pericentrin gene (PCNT) in a series of 24 Seckel/microcephalic osteodysplastic primordial dwarfism type II (MOPD II) families. *Journal of medical genetics* 47: 797–802.
- Nam EA, Cortez D (2011) ATR signalling: more than meeting at the fork. *The Biochemical journal* 436: 527–536.
- Zou L, Elledge SJ (2003) Sensing DNA damage through ATRIP recognition of RPA-ssDNA complexes. *Science* 300: 1542–1548.
- Ciccica A, Elledge SJ (2010) The DNA damage response: making it safe to play with knives. *Mol Cell* 40: 179–204.

19. Cortez D, Guntuku S, Qin J, Elledge SJ (2001) ATR and ATRIP: partners in checkpoint signaling. *Science* 294: 1713–1716.
20. Namiki Y, Zou L (2006) ATRIP associates with replication protein A-coated ssDNA through multiple interactions. *Proceedings of the National Academy of Sciences of the United States of America* 103: 580–585.
21. Ball HL, Myers JS, Cortez D (2005) ATRIP binding to replication protein A-single-stranded DNA promotes ATR-ATRIP localization but is dispensable for Chk1 phosphorylation. *Molecular biology of the cell* 16: 2372–2381.
22. Paciotti V, Clerici M, Lucchini G, Longhese MP (2000) The checkpoint protein Ddc2, functionally related to *S. pombe* Rad26, interacts with Mec1 and is regulated by Mec1-dependent phosphorylation in budding yeast. *Genes Dev* 14: 2046–2059.
23. Lakin ND, Jackson SP (1999) Regulation of p53 in response to DNA damage. *Oncogene* 18: 7644–7655.
24. Ward IM, Chen J (2001) Histone H2AX is phosphorylated in an ATR-dependent manner in response to replicational stress. *J Biol Chem* 276: 47759–47762.
25. Alderton GK, Joenje H, Varon R, Borghum AD, Jeggo PA, et al. (2004) Seckel syndrome exhibits cellular features demonstrating defects in the ATR signaling pathway. *Human Molecular Genetics* 13: 3127–3138.
26. Toledo LI, Murga M, Zur R, Soria R, Rodriguez A, et al. (2011) A cell-based screen identifies ATR inhibitors with synthetic lethal properties for cancer-associated mutations. *Nature structural & molecular biology* 18: 721–727.
27. Chanoux RA, Yin B, Urtishak KA, Asare A, Bassing CH, et al. (2009) ATR and H2AX cooperate in maintaining genome stability under replication stress. *The Journal of biological chemistry* 284: 5994–6003.
28. Andreassen PR, D'Andrea AD, Taniguchi T (2004) ATR couples FANCD2 monoubiquitination to the DNA damage response. *Genes and Development* 18: 1958–1963.
29. Noensie EN, Dietz HC (2001) A strategy for disease gene identification through nonsense-mediated mRNA decay inhibition. *Nature biotechnology* 19: 434–439.
30. Falck J, Coates J, Jackson SP (2005) Conserved modes of recruitment of ATM, ATR and DNA-PKcs to sites of DNA damage. *Nature* 434: 605–611.
31. Klingseisen A, Jackson AP (2011) Mechanisms and pathways of growth failure in primordial dwarfism. *Genes & development* 25: 2011–2024.
32. Murga M, Bunting S, Montana MF, Soria R, Mulero F, et al. (2009) A mouse model of ATR-*Seckel* shows embryonic replicative stress and accelerated aging. *Nature genetics* 41: 891–898.
33. Guernsey DL, Matsuoka M, Jiang H, Evans S, Macgillivray C, et al. (2011) Mutations in origin recognition complex gene *ORC4* cause Meier-Gorlin syndrome. *Nat Genet* 43: 360–364.
34. de Munnik SA, Bicknell LS, Aftimos S, Al-Aama JY, van Bever Y, et al. (2012) Meier-Gorlin syndrome genotype-phenotype studies: 35 individuals with pre-replication complex gene mutations and 10 without molecular diagnosis. *European journal of human genetics : EJHG* 20: 598–606.

Mutations in *UVSSA* cause UV-sensitive syndrome and impair RNA polymerase II processing in transcription-coupled nucleotide-excision repair

Yuka Nakazawa^{1-3,16}, Kensaku Sasaki^{4,16}, Norisato Mitsutake^{1,3,16}, Michiko Matsuse^{1,3}, Mayuko Shimada¹⁻³, Tiziana Nardo⁵, Yoshito Takahashi⁶, Kaname Ohyama^{1,7}, Kosei Ito^{1,8}, Hiroyuki Mishima⁴, Masayo Nomura⁴, Akira Kinoshita^{1,4}, Shinji Ono⁴, Katsuya Takenaka⁹, Ritsuko Masuyama⁸, Takashi Kudo¹⁰, Hanoch Slor¹¹, Atsushi Utani¹², Satoshi Tateishi¹³, Shunichi Yamashita^{3,14}, Miria Stefanini⁵, Alan R Lehmann¹⁵, Koh-ichiro Yoshiura⁴ & Tomoo Ogi¹⁻³

UV-sensitive syndrome (UV^SS) is a genodermatosis characterized by cutaneous photosensitivity without skin carcinoma¹⁻⁴. Despite mild clinical features, cells from individuals with UV^SS, like Cockayne syndrome cells, are very UV sensitive and are deficient in transcription-coupled nucleotide-excision repair (TC-NER)^{2,4,5}, which removes DNA damage in actively transcribed genes⁶. Three of the seven known UV^SS cases carry mutations in the Cockayne syndrome genes *ERCC8* or *ERCC6* (also known as *CSA* and *CSB*, respectively)^{7,8}. The remaining four individuals with UV^SS, one of whom is described for the first time here, formed a separate UV^SS-A complementation group^{1,9,10}; however, the responsible gene was unknown. Using exome sequencing¹¹, we determine that mutations in the *UVSSA* gene (formerly known as *KIAA1530*) cause UV^SS-A. The *UVSSA* protein interacts with TC-NER machinery and stabilizes the ERCC6 complex; it also facilitates ubiquitination of RNA polymerase II stalled at DNA damage sites. Our findings provide mechanistic insights into the processing of stalled RNA polymerase and explain the different clinical features across these TC-NER-deficient disorders.

We performed exome sequencing on two cell lines, Kps3 and XP24KO, derived from two individuals with UV^SS-A (cell lines described in Supplementary Table 1; exome described in Table 1, Online Methods, Supplementary Table 2a-c and Supplementary Note).

Using a recessive model of inheritance, we directly identified overlapping mutations in *KIAA1530* (NCBI Gene 57654), a predicted gene at 4p16.3 encoding a 709 amino acid protein of unknown function (Table 1 and Supplementary Table 2c). *KIAA1530* was subsequently renamed *UVSSA* (encoding UV-stimulated scaffold protein A) because of this finding, with support from the Human Gene Nomenclature Committee (HGNC). Affected individuals were homozygous for a c.367A>T mutation, which led to the introduction of a premature stop codon, p.Lys123*, in the *UVSSA* protein (Fig. 1a,b). We identified the same homozygous mutation in subject Kps2 (a sibling of Kps3) and a homozygous c.87delG mutation causing a p.Ile31Phefs*9 frameshift alteration in Israeli subject UV^SS24TA (Fig. 1b,c, Supplementary Fig. 1 and Supplementary Note). The identified mutations are summarized (Fig. 1d). We did not detect the 80-kDa *UVSSA* protein in any of the individuals with UV^SS-A (Fig. 1e). We also examined several mild xeroderma pigmentosum cases; in one case, XP70TO¹² (Supplementary Table 1), we identified a homozygous missense mutation (encoding p.Cys32Arg) in *UVSSA* (Fig. 1c,d), which implies that XP70TO is also in the UV^SS-A complementation group. The mutant protein was stably expressed in XP70TO cells, although band intensity was faint (Fig. 1f and Supplementary Fig. 2a-d).

The mutated allele encoding p.Lys123* was observed in the heterozygous state in 1 of 576 control individuals (allele frequency of 0.09%) evaluated by direct sequencing or high-resolution melting

¹Nagasaki University Research Centre for Genomic Instability and Carcinogenesis (NRGIC), Nagasaki, Japan. ²Department of Molecular Medicine, Atomic Bomb Disease Institute, Graduate School of Biomedical Sciences, Nagasaki University, Nagasaki, Japan. ³Department of Radiation Medical Sciences, Atomic Bomb Disease Institute, Graduate School of Biomedical Sciences, Nagasaki University, Nagasaki, Japan. ⁴Department of Human Genetics, Atomic Bomb Disease Institute, Graduate School of Biomedical Sciences, Nagasaki University, Nagasaki, Japan. ⁵Istituto di Genetica Molecolare, Consiglio Nazionale delle Ricerche, Pavia, Italy. ⁶Innovative Beauty Science Laboratory, Kanebo Cosmetics Inc., Odawara, Japan. ⁷Department of Environmental and Pharmaceutical Sciences, Graduate School of Biomedical Sciences, Nagasaki University, Nagasaki, Japan. ⁸Department of Cell Biology, Graduate School of Biomedical Sciences, Nagasaki University, Nagasaki, Japan. ⁹Department of Molecular Genetics, Medical Research Institute, Tokyo Medical and Dental University, Tokyo, Japan. ¹⁰Department of Radioisotope Medicine, Atomic Bomb Disease Institute, Graduate School of Biomedical Sciences, Nagasaki University, Nagasaki, Japan. ¹¹Human Molecular Genetics and Biochemistry, Sackler School of Medicine, Tel Aviv University, Tel Aviv, Israel. ¹²Department of Dermatology, Graduate School of Biomedical Sciences, Nagasaki University, Nagasaki, Japan. ¹³Institute of Molecular Embryology and Genetics, Kumamoto University, Kumamoto, Japan. ¹⁴Fukushima Medical University, Fukushima, Japan. ¹⁵Genome Damage and Stability Centre, University of Sussex, Brighton, UK. ¹⁶These authors contributed equally to this work. Correspondence should be addressed to T.O. (togi@nagasaki-u.ac.jp).

Received 26 September 2011; accepted 29 February 2012; published online 1 April 2012; doi:10.1038/ng.2229



Table 1 Direct identification of the UV^SS-A causal gene by exome sequencing of subjects Kps3 and XP24KO

Filter	Kps3	XP24KO
Single-nucleotide variants (SNVs)		
Total SNVs identified	75,368	94,628
Nonsynonymous missense, stop-gain, stop-loss, or splice-site ^a variants	7,161	6,904
Not reported in dbSNP131	383	340
Not reported in dbSNP131 or 1000 GP ^b	231	210
Not reported in dbSNP131, 1000 GP ^b or 7 control exomes ^c (new functionally significant SNVs)	217	202
Insertion and/or deletions (indels)		
Total indels identified	15,966	19,665
Frameshift indels, in-frame stop-gain, in-frame stop-loss or splice-site ^a variants	327	307
Not reported in dbSNP131	198	172
Not reported in dbSNP131 or 1000 GP ^b	85	76
Not reported in dbSNP131, 1000 GP ^b or 7 control exomes ^c (new functionally significant indels)	46	41
New functionally significant variants		
New SNVs or indels	263	243
Candidate genes under a recessive model		
Homozygous	9	17
Compound heterozygous	9	6
Potential causative genes shared among the subjects ^d	1 (<i>UVSSA</i>)	

The number of variants or genes that meet the criteria is indicated for each subject.

^aSplice-site acceptor or donor variants within 2 bp of exon-intron boundaries. ^b1000 Genomes Project full Phase 1 data, November 2010. ^cSeven Japanese in-house exome sequences. ^dUnder a recessive model, only one candidate gene, *UVSSA*, was identified.

analysis (HRMA) (**Supplementary Fig. 3a**); the mutations encoding p.Ile31Phefs*9 and p.Cys32Arg were not detected. Haploinsufficiency for *UVSSA* was negligible, as the parents of Kps2 and Kps3 showed no symptoms⁴. In parallel with exome sequencing, we performed

whole-genome SNP genotyping to identify runs of homozygosity (ROHs) shared among the affected individuals. We identified three overlapping ROHs (of >1 Mb) on autosomes, one of which encompassed the *UVSSA* locus (**Fig. 1g**, **Supplementary Fig. 3b,c** and

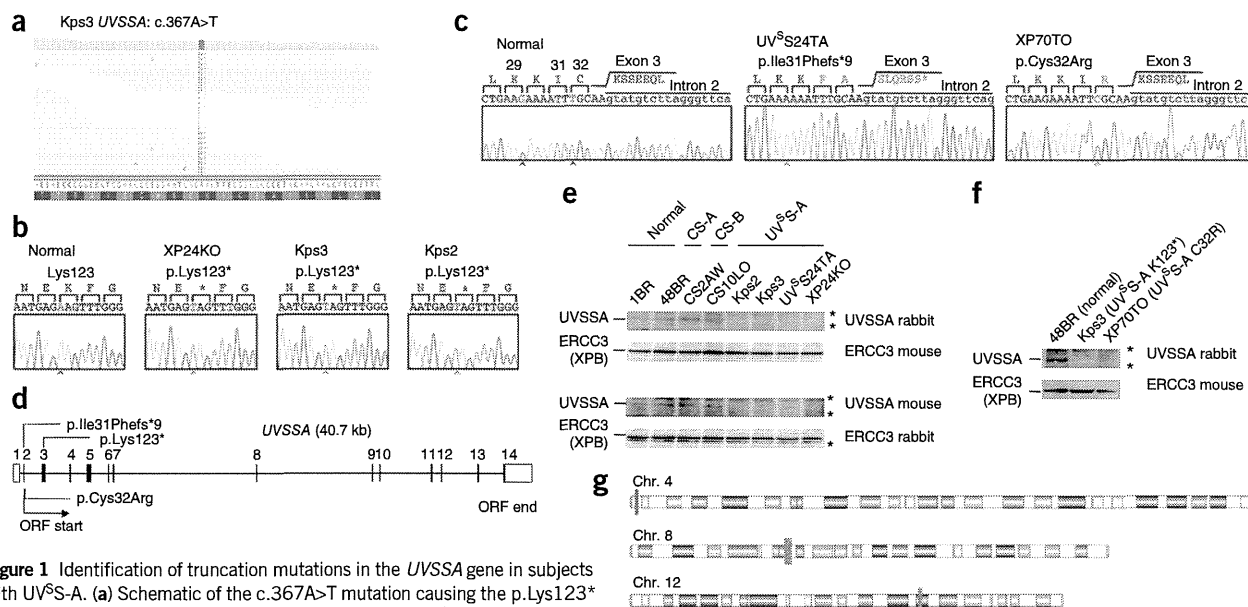


Figure 1 Identification of truncation mutations in the *UVSSA* gene in subjects with UV^SS-A. (a) Schematic of the c.367A>T mutation causing the p.Lys123* premature stop codon identified in subject Kps3 with UV^SS-A.

Exome-sequencing data were aligned, and individual reads are shown as beige lines; the position of the A-to-T substitution is in red. (b) Capillary Sanger sequencing showed that subjects XP24KO and Kps3 with UV^SS-A are homozygous for the c.367A>T SNV in *UVSSA* exon 3; the same mutation was also found in Kps2, the sibling of Kps3. The altered amino acid, Lys 123, is in red. (c) The c.87delG frameshift mutation and the p.Cys32Arg missense mutation were identified in subjects UV^SS24TA and XP70TO with UV^SS-A, respectively. Electropherograms of *UVSSA* exon 2 (uppercase) and intron 2 (lowercase) are shown. The deletion in the third position of the codon for Lys29 causes the p.Ile31Phefs*9 premature stop codon; the transition in the first position of the codon for Cys32 causes the p.Cys32Arg change (in red). Arrowheads indicate the position of the mutations. (d) The genomic structure of the *UVSSA* gene and the positions of the alterations in the subjects with UV^SS-A. (e,f) Immunoblots showing the 80-kDa *UVSSA* gene product in normal and Cockayne syndrome cells, which is missing in the UV^SS-A cells analyzed (e). *UVSSA* protein expression is reduced in XP70TO cells (f). ERCC3 is a loading control. 48BR and 1BR, normal cells; CS2AW, CS-A cells; CS10LO, CS-B cells; Kps2, Kps3, UV^SS24TA, XP24KO and XP70TO, UV^SS-A cells. Asterisks indicate nonspecific bands. (g) Shared ROH segments between subjects XP24KO, Kps3, Kps2 and UV^SS24TA with UV^SS-A. ROHs overlapping in all four subjects are shown as blue bars, and the overlapping region that contains the *UVSSA* gene is shown as a red bar (see **Supplementary Fig. 3b** for ROHs identified in the individual subjects and **Supplementary Fig. 3c** for a magnified view of the overlapped region found in chromosome 4).

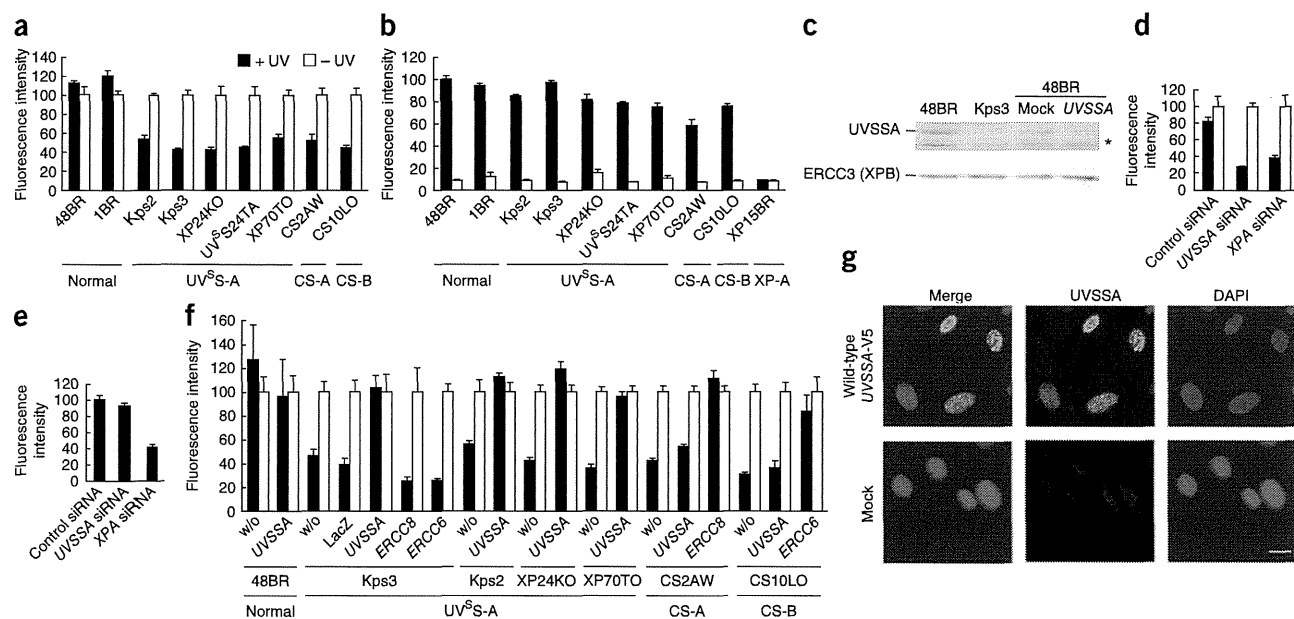


Figure 2 RNA synthesis recovery after UV irradiation requires *UVSSA* gene expression. (a) RRS activity after UV irradiation was reduced in the UV^S-A cells (filled bars, 10 J/m² of 254 nm UV-C; open bars, no UV). (b) Close-to-normal UDS activity in the UV^S-A cells (filled bars, 20 J/m² of UV-C; open bars, no UV). (c) *UVSSA* gene expression was diminished by siRNA. Normal 48BR cells were mock transfected or transfected with siRNA targeting *UVSSA*. Knockdown efficiency was detected by immunoblotting of the *UVSSA* protein, with ERCC3 as a loading control. The asterisk indicates a nonspecific band. (d) RRS activity after UV irradiation was completely abolished by abrogation of *UVSSA* gene expression. Normal 48BR cells were mock transfected or transfected with siRNA targeting *UVSSA* or *XPA* (filled bars, 10 J/m² of UV-C; open bars, no UV). (e) UDS activity was unaffected by siRNA knockdown of *UVSSA* (filled bars, 10 J/m² of UV-C; open bars, no UV). (f, g) Ectopic expression of wild-type *UVSSA* cDNA in UV^S-A cells by recombinant lentivirus infection completely rescued the RRS deficiency (filled bars, 10 J/m² of UV-C; open bars, no UV) (f). Viral infection efficiency (>85%) was confirmed by immunofluorescent staining of V5-tagged *UVSSA* protein (g). Scale bar, 20 μm. In a, d, f, RRS was normalized to activity in non-irradiated cells. UDS activity were normalized to that of normal 48BR cells in b or to that in cells mock transfected with siRNA in e. Error bars, s.d. of medians of nuclear fluorescence measurements in quintuplicate samples in a, b, d–f. w/o, without.

Supplementary Table 3a,b. No chromosome copy-number variation was detected (Supplementary Fig. 3d).

The findings strongly suggest that the mutations in *UVSSA* in the subjects with UV^S-A are causal for the disease; therefore, we next examined NER activities in the UV^S-A cells (Fig. 2). Unscheduled DNA synthesis (UDS¹³; defective in xeroderma pigmentosum) was nearly normal; however, RNA synthesis recovery (RRS¹⁴; defective in UV^S and in Cockayne syndrome) was diminished in all cell lines with mutated *UVSSA* (Fig. 2a,b; UDS and RRS were measured using a recently developed rapid, nonradioactive system^{15,16}). Similarly, small interfering RNA (siRNA)-based depletion of *UVSSA* transcripts (Fig. 2c) caused a marked reduction in RRS (Fig. 2d and Supplementary Fig. 4), whereas UDS was unaffected (Fig. 2e). Ectopic expression of wild-type *UVSSA* cDNA in UV^S-A cells restored normal RRS (Fig. 2f; V5-tagged *UVSSA* immunofluorescent staining shown in Fig. 2g), whereas it did not affect RRS in normal, CS-A or CS-B cells; neither *ERCC8* and *ERCC6* cDNA expression in UV^S-A cells restored RRS. We conclude that *UVSSA* is the causal gene for UV^S-A.

Mutations in the *ERCC8* and *ERCC6* genes underlie both Cockayne syndrome and UV^S7,8. To evaluate whether *UVSSA* mutations may also result in Cockayne syndrome phenotypes, we sequenced the *UVSSA* gene in 61 individuals with Cockayne syndrome whose genetic cause had not yet been determined (Supplementary Table 4). We found no obvious mutations, except for four new heterozygous changes. These changes, as well as the SNPs that were also found in control individuals and in persons with UV^S-A, did not affect RRS activity (Supplementary Fig. 5). These data

suggest that *UVSSA* function is distinct from that of genes involved in Cockayne syndrome (Supplementary Note).

Amino-acid sequences encoded by human *UVSSA* and its orthologs have no obvious similarity to other protein families. A domain of unknown function, DUF2043 (EMBL-EBI IPR018610) is located near the C terminus (Fig. 3a). We performed three-dimensional structure prediction using the PHYRE web server¹⁷ and identified a motif of 143–163 amino acids near the N terminus, which had substantial homology with the Vps-27, Hrs and STAM (VHS) domain¹⁸ (Fig. 3a and Supplementary Fig. 6a,b). VHS domain proteins have recently been implicated in ubiquitin binding¹⁹. A crystallographic study determined that Trp26, located in the α2 helix of the VHS domain of STAM1, interfaces with Ile44 of ubiquitin²⁰ (Supplementary Fig. 6c). Cys32 in *UVSSA* is located in the corresponding α2 helix (Supplementary Fig. 6b), and the p.Cys32Arg mutation can be superimposed onto the structure of the STAM1-ubiquitin complex, indicating that the Arg32 residue in the mutant *UVSSA* protein is oriented in the same direction as Trp26 in STAM1 (Supplementary Fig. 6d). These findings suggest that the p.Cys32Arg change in *UVSSA* that occurs in subject XP70TO may obstruct interactions between the VHS domain and ubiquitinated proteins.

To investigate the importance of the DUF2043 and VHS domains in TC-NER, we transduced *UVSSA* truncation mutants into UV^S-A cells and assayed complementation of the RRS defect (Fig. 3b). None of the truncation mutants lacking either the VHS or DUF2043 domain was able to restore RRS activity in these cells (Fig. 3c, Supplementary Fig. 7a (note that mutants T1 and T3 were unstable) and Supplementary Fig. 7b).

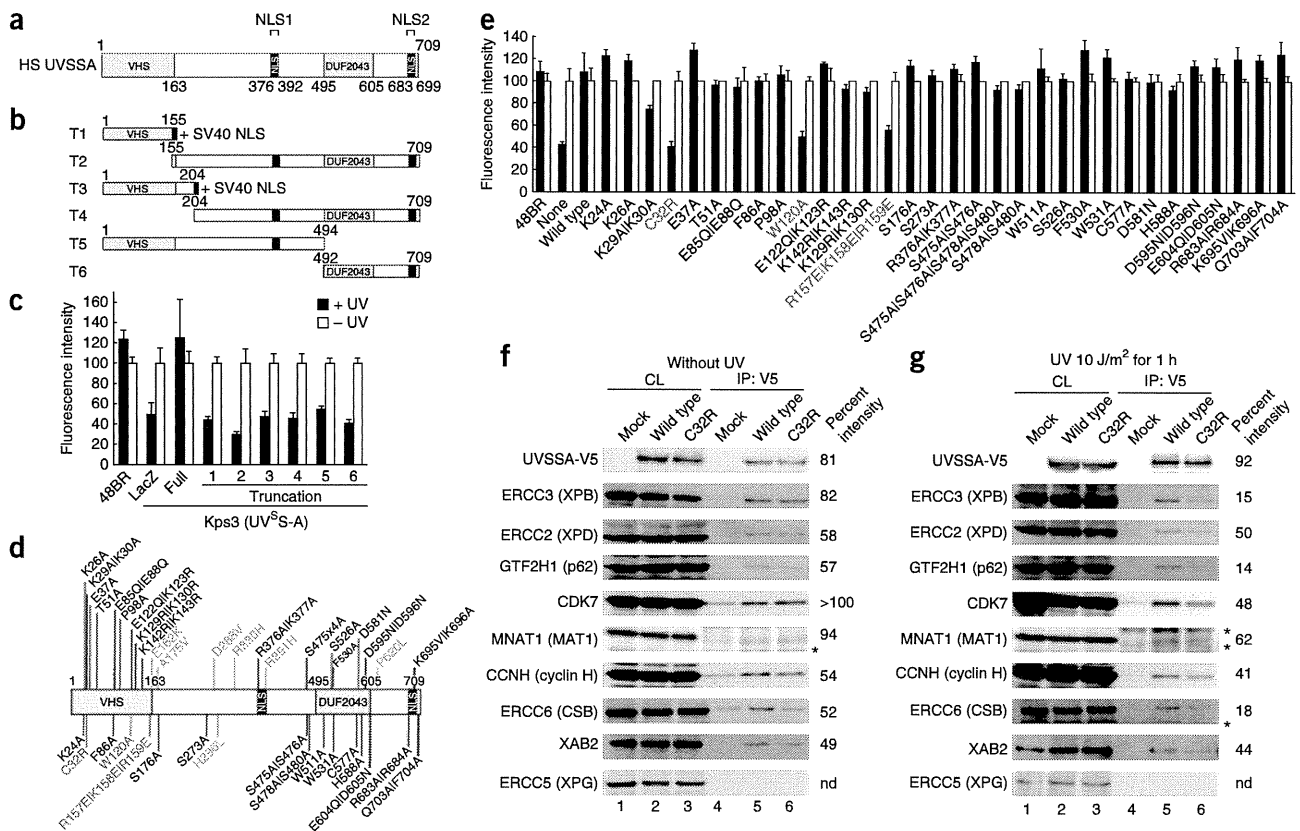


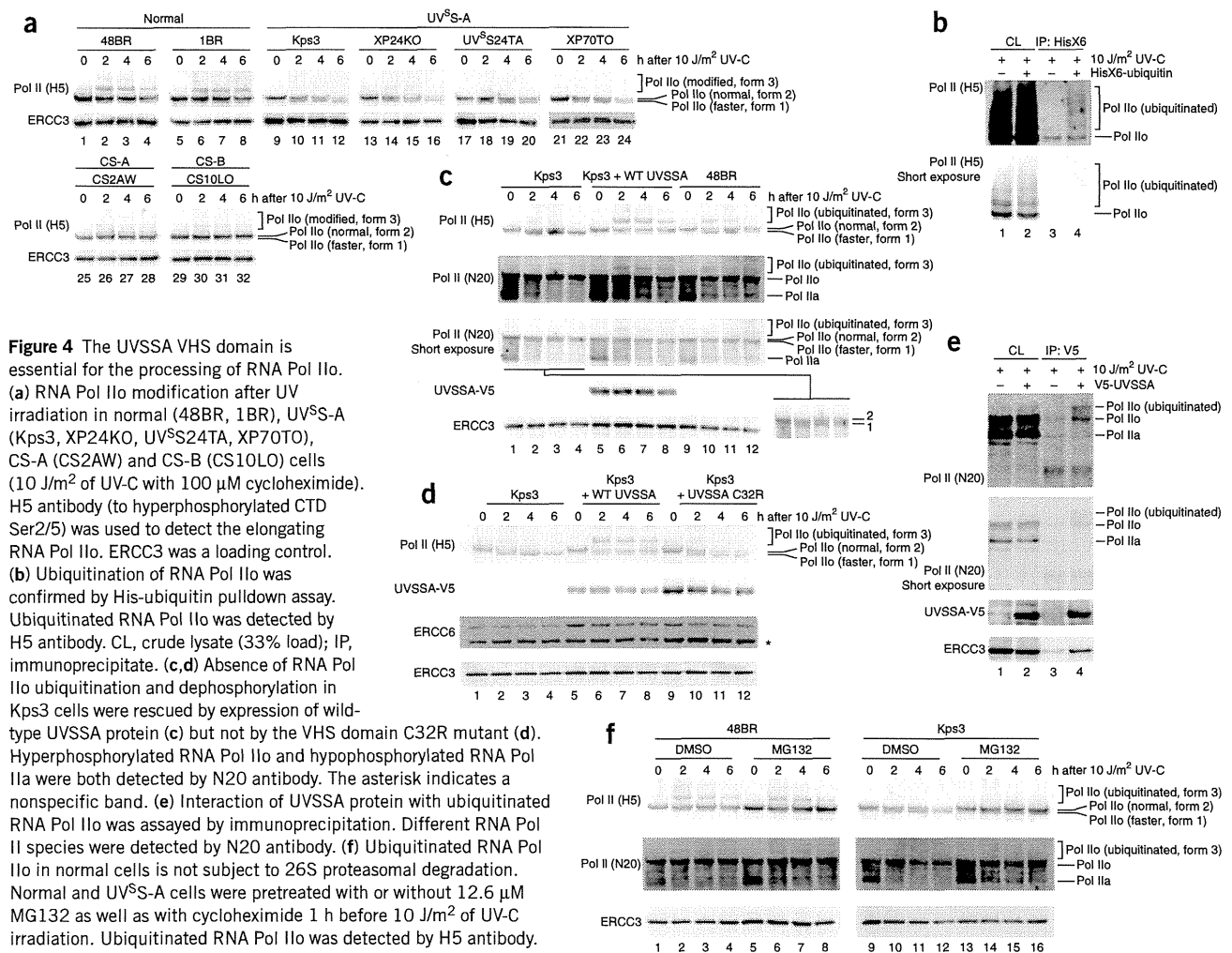
Figure 3 The N-terminal VHS domain of the UVSSA protein is essential for RRS activity and TFIH interaction. **(a,b)** Schematic of human full-length UVSSA **(a)** and UVSSA truncation mutants **(b)** used for the RRS assays. NLS1 and NLS2, putative nuclear-localization signals; T1–T6, truncation mutants. In T1 and T3, the SV40 NLS was added to the C terminus of the mutants. **(c)** RRS was measured in Kps3 cells expressing an intact (full) or truncated (T1–T6) form of V5-tagged UVSSA in **b** (filled bars, 10 J/m² of UV-C; open bars, no UV). **(d)** Schematic of the UVSSA mutants that were used for the RRS assays. Heterozygous alterations identified in individuals with Cockayne syndrome are shown in blue (see details in **Supplementary Table 4**); nonsynonymous SNPs found in normal, control individuals are shown in orange; changes shown in black and red are the amino-acid substitutions at residues conserved from Nematoda to humans as well as the XP70TO disease-causing mutation p.Cys32Arg. The three mutants shown in red did not complement the RRS deficiency of Kps3 cells. **(e)** RRS was measured in Kps3 cells expressing UVSSA mutants in **d** (filled bars, 10 J/m² of UV-C; open bars, no UV) (see also **Supplementary Fig. 5**). Expression of wild-type or mutant UVSSA in Kps3 cells was confirmed by immunofluorescent staining of V5-tagged protein (transfection efficiency was >85%; **Supplementary Figs. 7a,b** and **9**). In **c,e**, RRS activity was normalized to that in non-irradiated cells. Error bars, s.d. of medians of nuclear fluorescence measurements in quintuplicate samples. **(f,g)** Wild-type and UVSSA C32R protein interactions with NER factors were assayed by immunoprecipitation without irradiation **(f)**. The same interactions were assayed 1 h after 10 J/m² of UV irradiation **(g)**. Interactions were detected by immunoblotting with antibodies to the V5 tag (UVSSA), core TFIH factors (ERCC3, ERCC2, GTF2H1), CAK components (CDK7, CCNH, MNAT1) and ERCC6, XAB2 and ERCC5. CL, crude lysate (33% load); IP, immunoprecipitate. The intensities of the bands corresponding to factors binding to the mutant proteins are expressed as the percentages of that of the wild-type protein. Asterisks indicate nonspecific bands.

Next, we mutated residues conserved from Nematoda to humans (**Fig. 3d** and **Supplementary Fig. 8**). We found that, out of 32 mutants, only 3 carrying amino-acid changes to the 5 conserved residues located in the VHS domain (p.Cys32Arg, p.Trp120Ala and p.[Arg157Glu; Lys158Glu; Arg159Glu]) failed to restore normal RRS (**Fig. 3e** and **Supplementary Fig. 9**). Although we could not determine the critical amino-acid residues responsible for DUF2043 function, overall these findings indicate that the ubiquitin-binding VHS domain and the DUF2043 domain of UVSSA are crucial for TC-NER activity.

We next examined the association of UVSSA with TC-NER factors by immunoprecipitation. UVSSA interacted with several subunits of the core general transcription factor IIH (TFIIH) subcomplex (ERCC3 (also called XPB or p89), ERCC2 (also called XPD) and GTF2H1 (also called p62)) and the cyclin-dependent kinase (CDK) activating kinase (CAK) subcomplex (CDK7, CCNH (also called cyclin H) and MNAT1 (also called MAT1)), as well as with ERCC6 and the XPA-binding protein XAB2 (**Fig. 3f**). No robust interaction

was observed between UVSSA and ERCC5 (also known as XPG). Similar interactions were also observed after UV irradiation (**Fig. 3g**). UVSSA is thus a new factor associated with the TC-NER complexes. The absence of ERCC5 protein in the TFIH–UVSSA complex seems to conflict with a report showing that ERCC5 is important for stabilizing TFIH²¹; this discrepancy could partly be explained by the possibility that ERCC5 and UVSSA may share the same binding interface of TFIH.

In non-irradiated cells, UVSSA binding capabilities were unaffected by mutations in the VHS domain (**Fig. 3f**, lane 6, and **Supplementary Fig. 10a**, lane 6). However, following UV irradiation, its interactions with some TFIH subunits, namely GTF2H1 and ERCC3, and with ERCC6 were substantially weakened by amino-acid substitutions in the VHS domain (**Fig. 3g**, lane 6, and **Supplementary Fig. 10b**, lane 6). These interactions were confirmed by reverse immunoprecipitation (**Supplementary Fig. 10c**). These data indicate that UVSSA interacts transiently with the NER machinery,



and the VHS domain specifically supports direct contact with the TFIIF core complex and ERCC6 after UV irradiation.

In TC-NER, stalled RNA polymerase II (RNA Pol II) first has to be displaced by backtracking or degradation to allow access of the NER machinery⁶. ERCC8 and ERCC6 complexes (also called CS protein complexes; defective in Cockayne syndrome) are essential to this process²². During this step of TC-NER, some of the elongating form of RNA Pol II (RNA Pol IIo), which is phosphorylated at Ser2 and Ser5 in the C-terminal domain (CTD), is ubiquitinated²³, although the precise function of this ubiquitination is not known. We examined RNA Pol IIo modifications after UV irradiation in the presence of cycloheximide in normal, Cockayne syndrome and UV^S-A cells (Fig. 4a). (TC-NER activity was unaffected by cycloheximide in the experimental conditions used (Supplementary Fig. 11)). In normal cells (Fig. 4a, lanes 1–8), a slow-migrating fraction of RNA Pol IIo was observed after UV irradiation, and this modified band (form 3) decreased in intensity over time. Form 3 was not detected in normal cells after induction of oxidative DNA damage by treatment with hydrogen peroxide (Supplementary Fig. 12), suggesting that the modification is a UV damage-specific event. We confirmed that the RNA Pol IIo modification was ubiquitination as reported previously²³ (Fig. 4b). In contrast, in the UV^S cells, the ubiquitinated band was barely detectable, but a fast-migrating form of RNA Pol IIo (form 1) was observed, and the normally migrating form 2 decreased in intensity

over the 6-h period after irradiation (Fig. 4a, lanes 9–24). In the CS2AW (CS-A) or CS10LO (CS-B) cells (Fig. 4a, lanes 25–32), neither ubiquitination (see also ref. 23) nor form 1 was detected. Transduction of wild-type UVSSA cDNA into UV^S-A Kps3 cells restored the ubiquitination of RNA Pol IIo after UV irradiation (Fig. 4c, H5 in lanes 5–8). UVSSA overexpression was also associated with a substantial reduction in the levels of form 1 after UV irradiation (Fig. 4c, compare H5 in lanes 5–8 and 1–4, see also Fig. 4c, N20 (short exposure) in lanes 1–4 and its stretched image on the right (form 1–form 2 doublets are visible, regardless of the antibodies used)).

During transcription, RNA Pol IIo is eventually dephosphorylated to RNA Pol IIa to recycle RNA Pol II for another round of transcription initiation. In TC-NER, displaced RNA Pol IIo is also dephosphorylated and recycled (Fig. 4c, N20 in lanes 9–12). Dephosphorylation was substantially inhibited in UV^S-A cells 4–6 h after UV irradiation (Fig. 4c, N20 in lanes 1–4), as previously reported for Cockayne syndrome cells²⁴, and was restored following expression of UVSSA cDNA (Fig. 4c, N20 in lanes 5–8). RNA Pol IIo ubiquitination was not restored in Kps3 cells by expression of mutants with amino-acid substitutions in the VHS domain (Fig. 4d, H5 in lanes 9–12, and Supplementary Fig. 13, H5 in lanes 9–12), indicating that the VHS domain is crucial for RNA Pol IIo processing.

We noticed that ERCC6 protein was degraded in UV^S-A cells after UV irradiation, indicating that UVSSA contributes to the stabilization

of the ERCC6 complex in TC-NER (Fig. 4d, ERCC6 in lanes 1–4). The reduction of ERCC6 protein levels in Kps3 cells was restored following expression of either wild-type or VHS domain-mutated (p.Cys32Arg) UVSSA (Fig. 4d, ERCC6 in lanes 5–12, and Supplementary Fig. 14). These data indicate that the absence of RNA Pol II ubiquitination in the UV^S-A cells is not a side effect of Cockayne syndrome protein depletion (Fig. 2f; ectopic expression of ERCC6 did not restore RRS in UV^S-A cells). We further showed that UVSSA specifically binds to RNA Pol II and ubiquitinated RNA Pol II but not to RNA Pol IIa and that ubiquitinated RNA Pol II is enriched in the UVSSA-binding fraction (Fig. 4e).

These findings suggest that UVSSA recruits an E3 ubiquitin ligase and facilitates ubiquitination of RNA Pol II. K48-linked polyubiquitination triggers 26S proteasomal degradation of the targeted protein, whereas monoubiquitination and K63-linked polyubiquitination contribute to functional modifications of various DNA repair factors. The BRCA1-BARD1 complex and the NEDD4 E3 ubiquitin ligase, as well as the ERCC8 complex, have been reported to be involved in damage-dependent polyubiquitination and degradation of RNA Pol II^{25–27}. To determine whether RNA Pol II is degraded as a consequence of UVSSA-mediated ubiquitination, we analyzed RNA Pol II modifications after UV irradiation and subsequent treatment with the 26S proteasome inhibitor MG132 in normal and UV^S-A cells (Fig. 4f). The band corresponding to ubiquitinated form 3 of RNA Pol II did not increase substantially in intensity in normal cells treated with MG132 (Fig. 4f, compare H5 in lanes 1–4 and 5–8); conversely, increases in intensity for bands corresponding to the normal form 2 of RNA Pol II as well as to RNA Pol IIa were observed, both in normal and UV^S-A cells, in the presence of inhibitor (Fig. 4f, lanes 5–8 and 13–16). Taken together, these data indicate that UVSSA-dependent RNA Pol II ubiquitination is not subject to 26S proteasomal degradation and may therefore be K63 linked, although a substantial amount of stalled RNA Pol II is degraded by UVSSA-independent ubiquitination pathways. We speculate that the TFIIF core factor GTF2H2 (p44) is a candidate for an alternative E3 ubiquitin ligase²⁸, which may form stable K63-linked polyubiquitin chains on stalled RNA Pol II during TC-NER. Further studies will address this hypothesis. We conclude that UVSSA has an important role in the processing of RNA Pol II molecules stalled at sites of UV damage.

In conclusion, we have newly identified UVSSA as the gene causing UV-sensitive syndrome, and the UVSSA protein is involved in TC-NER of UV damage. UVSSA interacts with TFIIF, ERCC6 and RNA Pol II, and the VHS domain is indispensable for TC-NER activity and for ubiquitination and dephosphorylation in the processing of stalled RNA Pol II. We hypothesize that UVSSA directly recruits TFIIF at sites where RNA Pol II is stalled at UV damage (but not at oxidative damage sites; Supplementary Fig. 12)^{5,7,29} and facilitates RNA Pol II ubiquitination and promotes its backtracking to allow access to the NER machinery. We also found that UVSSA contributes to stabilization of the ERCC6 complex; in accompanying reports by Zhang *et al.*³⁰ and Schwertman *et al.*³¹, the UVSSA-USP7 complex is shown to be involved in the regulation of ERCC6 ubiquitination. These various UVSSA functions coordinate the removal of stalled RNA Pol II and formation of the TC-NER pre-incision complex to promote the subsequent steps of NER and transcription resumption at UV-damaged sites.

Cockayne syndrome but not UV^S cells are sensitive to oxidative DNA damage^{5,7,29,32}; this differential sensitivity could explain the difference between symptoms in the two syndromes. Our findings, however, suggest that aberrant RNA Pol II processing may also contribute to clinical outcome (Supplementary Fig. 15). RNA Pol II

stalled at DNA damage is normally stably ubiquitinated and backtracked in a process dependent on ERCC8 and ERCC6 complexes and UVSSA, facilitating removal of DNA damage and prompt transcription resumption (Supplementary Fig. 15a–d). In UV^S-A cells, stalled RNA Pol II can still be ubiquitinated in an alternative pathway that is dependent on ERCC8 and ERCC6 complexes and independent of UVSSA that leads to 26S proteasomal degradation of RNA Pol II, so that transcription resumption does not occur (Supplementary Fig. 15e,f). In individuals with Cockayne syndrome, neither of these pathways is operative (Supplementary Fig. 15h), suggesting that prolonged arrest of RNA Pol II at DNA lesions (leading to a signal for apoptosis)⁶, as in Cockayne syndrome cells, is more deleterious than degradation that occurs in UV^S-A cells, and this might contribute to the more severe clinical features in Cockayne syndrome relative to those in UV^S. UVSSA is thus a key factor that controls the fate of RNA Pol II stalled at DNA damage.

URLS. NRGIC, <http://www.nrgic.prj.nagasaki-u.ac.jp/>; NCBI, <http://www.ncbi.nlm.nih.gov/>; EMBL-EBI nucleotide sequence database, <http://www.ebi.ac.uk/embl/>; Phyre2, <http://www.sbg.bio.ic.ac.uk/phyre2/html/page.cgi?id=index>; Picard version 1.38, <http://picard.sourceforge.net/index.shtml>; UCSC Genome Bioinformatics, <http://genome.ucsc.edu/>; dbSNP Build 131, <http://www.ncbi.nlm.nih.gov/projects/SNP/>; 1000 Genomes Project full Phase 1 data, http://www.openbioinformatics.org/annovar/download/hg19_ALL.sites.2010_11.txt.gz; ANNOVAR, <http://www.openbioinformatics.org/annovar/>; SIFT dataset, http://www.openbioinformatics.org/annovar/download/hg19_avsift.txt.gz; NIPPON EGT (siRNA oligonucleotides), <http://www.n-egt.com/products/sirna/specification.html>; TaKaRa (qPCR primers), <http://www.takara-bio.co.jp/prt/intro.htm>.

METHODS

Methods and any associated references are available in the online version of the paper at <http://www.nature.com/naturegenetics/>.

Note: Supplementary information is available on the Nature Genetics website.

ACKNOWLEDGMENTS

We are grateful to P. Hanawalt and G. Spivak for their helpful comments on the manuscript. We are grateful to C. Hayashida, M. Kawamichi and H. Fawcett for technical assistance. This work was supported by Special Coordination Funds for Promoting Science and Technology from the Japan Science and Technology Agency (JST) (to Y.N., K.O., K.I., R.M. and T.O.), a grant-in-aid for Scientific Research KAKENHI (22710056) from the Japanese Society for the Promotion of Science, a science research grant from the Inamori Foundation, a cancer research grant from The Sagawa Foundation for Promotion of Cancer Research, a medical research grant from Mochida Memorial Funds for Medical and Pharmaceutical Research, a medical research grant from the Daiichi-Sankyo Foundation of Life Science, a medical research grant from the Takeda Science Foundation, a grant-in-aid for Seeds Innovation (Type-A) from JST (to T.O.), a Global Centers of Excellence (COE) Program from the Ministry of Education, Culture, Sports, Science and Technology of Japan (to Y.N., K.S., N.M., M.M., M. Shimada, S.Y., K.Y. and T.O.), grants from the Ministry of Health, Labour and Welfare (to K.Y.), the Associazione Italiana per la Ricerca sul Cancro (to M. Stefanini), a Medical Research Council (MRC) programme grant and an EC-RTN and integrated project (to A.R.L.).

AUTHOR CONTRIBUTIONS

N.M. and T.O. designed the study and experiments. Y.N., N.M., M.M., M. Shimada, T.N., K.O., K.I., K.T., R.M. and T.O. performed molecular and cell biology experiments. Y.N., K.S., M. Shimada, Y.T., M.N., A.K., S.O., K.Y. and T.O. performed genetic experiments. K.S., M. Shimada, Y.T., H.M., M.N., A.K., S.O., K.Y. and T.O. analyzed the genetic data. Y.T., H.S., A.U., S.T., M. Stefanini and A.R.L. contributed Cockayne syndrome and UV^S subject materials. N.M., Y.T., T.K., A.U., S.Y., M. Stefanini, A.R.L., K.Y. and T.O. coordinated the study. N.M., M. Stefanini, A.R.L. and T.O. wrote the manuscript. All authors commented on the manuscript.



COMPETING FINANCIAL INTERESTS

The authors declare no competing financial interests.

Published online at <http://www.nature.com/naturegenetics/>.

Reprints and permissions information is available online at <http://www.nature.com/reprints/index.html>.

- Spivak, G. UV-sensitive syndrome. *Mutat. Res.* **577**, 162–169 (2005).
- Itoh, T., Fujiwara, Y., Ono, T. & Yamaizumi, M. UVs syndrome, a new general category of photosensitive disorder with defective DNA repair, is distinct from xeroderma pigmentosum variant and rodent complementation group I. *Am. J. Hum. Genet.* **56**, 1267–1276 (1995).
- Fujiwara, Y., Ichihashi, M., Kano, Y., Goto, K. & Shimizu, K. A new human photosensitive subject with a defect in the recovery of DNA synthesis after ultraviolet-light irradiation. *J. Invest. Dermatol.* **77**, 256–263 (1981).
- Itoh, T., Ono, T. & Yamaizumi, M. A new UV-sensitive syndrome not belonging to any complementation groups of xeroderma pigmentosum or Cockayne syndrome: sibs showing biochemical characteristics of Cockayne syndrome without typical clinical manifestations. *Mutat. Res.* **314**, 233–248 (1994).
- Spivak, G. *et al.* Ultraviolet-sensitive syndrome cells are defective in transcription-coupled repair of cyclobutane pyrimidine dimers. *DNA Repair (Amst.)* **1**, 629–643 (2002).
- Hanawalt, P.C. & Spivak, G. Transcription-coupled DNA repair: two decades of progress and surprises. *Nat. Rev. Mol. Cell Biol.* **9**, 958–970 (2008).
- Nardo, T. *et al.* A UV-sensitive syndrome patient with a specific CSA mutation reveals separable roles for CSA in response to UV and oxidative DNA damage. *Proc. Natl. Acad. Sci. USA* **106**, 6209–6214 (2009).
- Horibata, K. *et al.* Complete absence of Cockayne syndrome group B gene product gives rise to UV-sensitive syndrome but not Cockayne syndrome. *Proc. Natl. Acad. Sci. USA* **101**, 15410–15415 (2004).
- Cleaver, J.E. & Thomas, G.H. Clinical syndromes associated with DNA repair deficiency and enhanced sun sensitivity. *Arch. Dermatol.* **129**, 348–350 (1993).
- Itoh, T., Linn, S., Ono, T. & Yamaizumi, M. Reinvestigation of the classification of five cell strains of xeroderma pigmentosum group E with reclassification of three of them. *J. Invest. Dermatol.* **114**, 1022–1029 (2000).
- Ng, S.B. *et al.* Targeted capture and massively parallel sequencing of 12 human exomes. *Nature* **461**, 272–276 (2009).
- Kawada, A., Satoh, Y. & Fujiwara, Y. Xeroderma pigmentosum complementation group E: a case report. *Photodermatol.* **3**, 233–238 (1986).
- Stefanini, M. *et al.* Genetic heterogeneity of the excision repair defect associated with trichothiodystrophy. *Carcinogenesis* **14**, 1101–1105 (1993).
- Mayne, L.V. & Lehmann, A.R. Failure of RNA synthesis to recover after UV irradiation: an early defect in cells from individuals with Cockayne's syndrome and xeroderma pigmentosum. *Cancer Res.* **42**, 1473–1478 (1982).
- Limsirichaikul, S. *et al.* A rapid non-radioactive technique for measurement of repair synthesis in primary human fibroblasts by incorporation of ethynyl deoxyuridine (EdU). *Nucleic Acids Res.* **37**, e31 (2009).
- Nakazawa, Y., Yamashita, S., Lehmann, A.R. & Ogi, T. A semi-automated non-radioactive system for measuring recovery of RNA synthesis and unscheduled DNA synthesis using ethynyluracil derivatives. *DNA Repair (Amst.)* **9**, 506–516 (2010).
- Kelley, L.A. & Sternberg, M.J. Protein structure prediction on the Web: a case study using the Phyre server. *Nat. Protoc.* **4**, 363–371 (2009).
- Lohi, O., Poussu, A., Mao, Y., Quijcho, F. & Lehto, V.P. VHS domain—a longshoreman of vesicle lines. *FEBS Lett.* **513**, 19–23 (2002).
- Dikic, I., Wakatsuki, S. & Walters, K.J. Ubiquitin-binding domains—from structures to functions. *Nat. Rev. Mol. Cell Biol.* **10**, 659–671 (2009).
- Ren, X. & Hurley, J.H. VHS domains of ESCRT-0 cooperate in high-avidity binding to polyubiquitinated cargo. *EMBO J.* **29**, 1045–1054 (2010).
- Ito, S. *et al.* XPG stabilizes TFIIH, allowing transactivation of nuclear receptors: implications for Cockayne syndrome in XP-G/CS patients. *Mol. Cell* **26**, 231–243 (2007).
- Fousteri, M., Vermeulen, W., van Zeeland, A.A. & Mullenders, L.H. Cockayne syndrome A and B proteins differentially regulate recruitment of chromatin remodeling and repair factors to stalled RNA polymerase II *in vivo*. *Mol. Cell* **23**, 471–482 (2006).
- Bregman, D.B. *et al.* UV-induced ubiquitination of RNA polymerase II: a novel modification deficient in Cockayne syndrome cells. *Proc. Natl. Acad. Sci. USA* **93**, 11586–11590 (1996).
- Rockx, D.A. *et al.* UV-induced inhibition of transcription involves repression of transcription initiation and phosphorylation of RNA polymerase II. *Proc. Natl. Acad. Sci. USA* **97**, 10503–10508 (2000).
- Anindya, R., Aygun, O. & Svejstrup, J.Q. Damage-induced ubiquitylation of human RNA polymerase II by the ubiquitin ligase Nedd4, but not Cockayne syndrome proteins or BRCA1. *Mol. Cell* **28**, 386–397 (2007).
- Starita, L.M. *et al.* BRCA1/BARD1 ubiquitinate phosphorylated RNA polymerase II. *J. Biol. Chem.* **280**, 24498–24505 (2005).
- Kleiman, F.E. *et al.* BRCA1/BARD1 inhibition of mRNA 3' processing involves targeted degradation of RNA polymerase II. *Genes Dev.* **19**, 1227–1237 (2005).
- Takagi, Y. *et al.* Ubiquitin ligase activity of TFIIH and the transcriptional response to DNA damage. *Mol. Cell* **18**, 237–243 (2005).
- Spivak, G. & Hanawalt, P.C. Host cell reactivation of plasmids containing oxidative DNA lesions is defective in Cockayne syndrome but normal in UV-sensitive syndrome fibroblasts. *DNA Repair (Amst.)* **5**, 13–22 (2006).
- Zhang, X. *et al.* Mutations in UVSSA cause UV-sensitive syndrome and destabilize ERCC6 in transcription-coupled DNA repair. *Nat. Genet.* published online (1 April 2012); doi:10.1038/ng.2228.
- Schwertman, P. *et al.* UV-sensitive syndrome protein UVSSA recruits USP7 to regulate transcription-coupled repair. *Nat. Genet.* published online (1 April 2012); doi:10.1038/ng.2230.
- D'Errico, M. *et al.* The role of CSA in the response to oxidative DNA damage in human cells. *Oncogene* **26**, 4336–4343 (2007).



ONLINE METHODS

Human studies. Samples from affected individuals and controls were obtained with local ethical approval (Nagasaki University Ethical, Legal and Social Implications (ELSI) committee). Written informed consent was obtained from the subjects.

Exome sequencing. Genomic DNA of affected individuals (Kps3 and XP24KO) was enriched using the Agilent SureSelect Human All Exon Kit (Agilent, G3362), according to the manufacturer's instructions. The kit covers 1.22% of human genomic regions, which correspond to the CCDS exons. Briefly, genomic DNA was fragmented (~150–200 bp) and ligated to the Illumina sequencing adaptor oligonucleotides. The adaptor-ligated fragments were then amplified by ligation-mediated PCR (LM-PCR) and were then hybridized to the SureSelect Biotinylated RNA library for exon enrichment. The hybridized fragments were captured by streptavidin-coated magnetic beads. The captured genomic fragments were sequenced on a single lane of the Illumina Genome Analyzer IIx (GAIIx) sequencer using 75-bp paired-end reads.

Bioinformatic analysis for the exome data. Low-quality sequences of each read end were filtered out (Supplementary Table 2a). In this study, low-quality sequences were defined as reads that contained more than six unknown bases or >40 continuous identical bases or those contaminated by adaptor sequences during the capture and sequencing steps. The filtered sequences were aligned to the human reference genome (GRCh37/hg19) with the Burrows-Wheeler Aligner (BWA) version 0.5.8 (ref. 33) (Supplementary Table 2a). Picard version 1.38 was used to convert, sort and index the aligned data files. Picard was also used to identify and remove duplicate reads from the samples. Base-quality scores were recalibrated, and sequence reads were locally realigned with the Genome Analysis Toolkit (GATK) version 1.0.4905 (refs. 34,35). SNVs were identified by the Unified Genotyper program in GATK (Supplementary Table 2b). Low-quality variants were then filtered out using the Variant Filtration Walker tools in GATK if they met the following criteria: (i) SNV clustering and proximity to indels, (ii) confidence (QUAL) score of <30, (iii) greater than 10% of aligned reads at a site with mapping quality of 0 (MAPQ0), (iv) strand-bias score of >–0.1, (v) quality-over-depth score of <5 or (vi) largest contiguous homopolymer run of variant allele in either direction (HRun) of >5. Small indels were detected with the detection of indels (Dindel) program, according to the basic procedure for calling indels from a diploid sample in the Dindel user guide version 1.0 (ref. 36). We filtered out any indels matching the following criteria: (i) quality score of <20, (ii) reference homopolymer length of >10 or (iii) indel allele not covered by at least one read on both strands. All variants were annotated with ANNOVAR³⁷. Annotation of variants was based on NCBI and UCSC databases. Variants identified in the following SNP databases were removed: dbSNP (Build 131), the 1000 Genomes Project full Phase 1 data that are based on variants from 629 individuals and seven in-house Japanese exome sequencing data sets (Table 1). The effect of each mutation was predicted using the Sorting Intolerant from Tolerant (SIFT) score³⁸ (Supplementary Table 2c). We obtained SIFT scores from the ANNOVAR-SIFT database. According to a recessive inheritance model, we selected genes that carried at least one new homozygous or more than two heterozygous changes in one gene locus (Table 1) (see Supplementary Note for further details).

Run-of-homozygosity (ROH) analysis. Whole-genome SNP genotyping of the subjects with UV^{SS}-A was performed on the Genome-Wide Human SNP Array 6.0 (Affymetrix), according to the manufacturer's instructions. The genotype data were generated using the birdseed v2 algorithm in the Genotyping Console 4.0 (Affymetrix). Homozygosity mapping and copy-number analysis were performed by the Partek Genomics Suite v6.5. We determined the runs of homozygosity (ROHs) of at least 1 Mb, allowing up to 1% error. The shared ROHs among the affected individuals were determined. Genomic positions of the identified SNPs were based on the human genome (GRCh37/hg19).

Quantitative RT-PCR analysis. mRNA from affected individuals was purified using the RNeasy mini kit (QIAGEN). cDNA was synthesized from mRNA using a mixture of oligo(dT) and random hexamer primers with the SuperScript II reverse transcription system (Invitrogen). UVSSA mRNA transcript levels in 48BR, Kps3 and XP70TO cells were determined by qRT-PCR assays using SYBR Premix Ex-TaqII polymerase (Perfect Real Time system, TaKaRa) and the Thermal Cycler Dice Real Time System II (TaKaRa). Transcripts from the *HPRT1* allele were used as a quantification control. Experiments were performed in triplicate, and qPCR results were analyzed by the $\Delta\Delta C_T$ method. The sequences of qPCR primers used for the assay can be obtained from the company website.

High-resolution melting analysis (HRMA). HRMA of UVSSA exons 2 and 3 in 576 unrelated Japanese control individuals (in house) was performed to determine the allele frequencies of the stop-gain SNVs p.Lys123* and p.Ile31Phefs*9 identified in the individuals with UV^{SS}-A. The HRMA profile was collected on the LightCycler 480 Real-Time PCR system (Roche). Melting curves were analyzed by LightCycler 480 Gene Scanning software (Roche).

Recovery of RNA synthesis (RRS) assays. Experimental details have been described previously¹⁶. Cells were plated in plastic 96-well plates. Virus infection was performed 48 h before RRS assays. Cells were UV irradiated (10 J/m² of 254 nm UV-C) and incubated for 12 h for RNA synthesis recovery. RRS was measured by the fluorescence-based ethynyluridine incorporation assay¹⁶. Briefly, recovered cells were incubated for 2 h in medium supplemented with 100 μ M 5-ethynyluridine followed by ethynyluridine detection with a copper-catalyzed fluorescent azide conjugation reaction (Click reaction). Cells were fixed and permeabilized in 2% paraformaldehyde and 0.5% Triton X-100 in PBS; after washing with PBS, cells were incubated with 15 μ M Alexa Fluor 488 azide (Invitrogen) in 50 mM Tris-HCl, pH 7.3, 4 mM CuSO₄, 10 mM sodium ascorbate and 20 ng/ml DAPI for 1 h. Cells were then washed with PBST (PBS with 0.05% Tween20). Nuclear fluorescent image acquisition and data processing were automated using the In-Cell-Analyzer system (GE Healthcare).

Unscheduled DNA synthesis (UDS) assays. Experimental details have been described previously^{15,16}. Cells were plated in 96-well plates. siRNA transfection was performed 72 h before UDS assays. UDS was measured by the fluorescence-based ethynyldeoxyuridine incorporation assay^{15,16}. Cells were UV irradiated (20 J/m² of 254 nm UV-C) and incubated for 4 h in medium supplemented with 5 μ M 5-ethynyl-2'-deoxyuridine (EdU). Incorporated EdU was detected by a copper-catalyzed fluorescent azide conjugation reaction (Click reaction). Nuclear fluorescent image acquisition and data processing were automated using the In-Cell-Analyzer system (GE Healthcare).

Immunofluorescence detection of UVSSA protein. Cells were plated in glass-bottomed 96-well plates. Lentivirus particles that expressed either wild-type UVSSA or series of mutant UVSSA proteins (V5 tagged) were used to infect cells 48 h before immunodetection. Cells were fixed and permeabilized in 2% paraformaldehyde and 0.2% Triton X-100 in PBS; after washing with PBS, cells were incubated with mouse antibody to V5 diluted 1:200 in PBST for 1 h and were extensively washed with PBST. Cells stained with primary antibody were then incubated for 1 h with DAPI (5 ng/ml) and a 1:1,000 dilution of rabbit antibody to mouse IgG conjugated with Alexa Fluor 488 (Molecular Probes). Cells were then washed with PBST. Photographs of the cells were captured with an AxioObserver Z1 microscope (Zeiss) equipped with a charge-coupled device (CCD) camera; captured images were analyzed with Axiovision software (Zeiss).

Coimmunoprecipitation. To investigate the interaction of the UVSSA protein with TC-NER factors, HEK293T cells were transfected with expression plasmids encoding V5-tagged UVSSA (wild type and the C32R and W120A



mutants) and incubated for 24 h. In reverse immunoprecipitation experiments, V5-tagged human ERCC3, GTF2H1, CDK7, ERCC6 and ERCC5 were used. Whole-cell lysates were prepared using the CelLytic Nuclear Extraction kit (Sigma). Coimmunoprecipitation was performed using rabbit antibody to V5 conjugated to agarose beads (MBL).

Immunoblotting. Whole-cell lysates and immunoprecipitated samples were resolved by SDS-PAGE (5–20% gradient gels). Resolved protein samples were transferred to PVDF membrane for immunodetection, unless otherwise noted.

Antibodies. Antibodies used for this study were rabbit polyclonal antibody to UVSSA raised against the N-terminal VHS domain of the human UVSSA protein (NBP1-32598, GeneTex), mouse polyclonal antibody to UVSSA raised against full-length human UVSSA protein (H00057654-B01, Abnova), mouse monoclonal antibody to the V5 tag (1H6, MBL), rabbit polyclonal antibody to the V5 tag (PM003, MBL), mouse monoclonal antibody to p89/ERCC3 (AB3, CRUK), rabbit polyclonal antibody to p89/ERCC3 (S-19, Santa Cruz Biotechnology), mouse monoclonal antibody to XPD/ERCC2 (2F6, CRUK), mouse monoclonal antibody to p62/GTF2H1 (G10, Santa Cruz Biotechnology), mouse monoclonal antibody to CDK7 (MO1, MBL), rabbit polyclonal antibody to MNAT1 (MAT1) (FL-309, Santa Cruz Biotechnology), mouse monoclonal antibody to CCNH (cyclin H) (1B8, Abnova), mouse monoclonal antibody to CSB/ERCC6 (553C5a, BMR), mouse monoclonal antibody to XAB2 (5-17, Santa Cruz Biotechnology), mouse monoclonal antibody to XPG/ERCC5 (8H7, CRUK); mouse monoclonal antibody to RNA polymerase II large subunit C-terminal domain Ser2 phosphorylated (H5, Covance), rabbit polyclonal antibody to RNA polymerase II (N20, Santa Cruz Biotechnology) and rabbit polyclonal antibody to p53 phosphorylated at Ser15 (Cell Signaling Technology).

Detection of the elongating RNA Pol IIo after UV irradiation. Cells were cultured in medium supplemented with 100 μ M cycloheximide for 1 h before UV irradiation. Cells were irradiated (10 J/m² of UV-C) and incubated for the indicated time periods in medium containing cycloheximide. Whole-cell lysates were resolved on 6% SDS-PAGE gels and transferred to PVDF membrane. RNA polymerase II in elongation mode (RNA Pol IIo) was detected with H5 antibody (to phosphorylated CTD-Ser2/5).

Ubiquitin pulldown assays. Crude lysates were prepared from HEK293T cells that were mock transfected or transfected with a plasmid encoding N-terminally 6 \times histidine-tagged ubiquitin. Cells were irradiated (10 J/m² of UV-C) and incubated for 1 h. Extracts were immunoprecipitated with agarose-conjugated antibody to the His tag. Ubiquitinated RNA Pol IIo was detected by H5 antibody.

siRNA experiments. siRNA oligonucleotides targeting UVSSA and XPA were purchased from Nippon EGT (sequences can be obtained from the company's

website). A mixture of three different siRNA oligonucleotides designed for different regions of each gene was used for all experiments, unless otherwise noted. Individual siRNA oligonucleotides were also used for the experiments presented in **Supplementary Figure 4**. siRNA transfection was performed using X-tremeGENE (Roche) transfection reagent, according to the manufacturer's instructions. In typical experiments, 10 nM of siRNA was transfected in suspension in a reverse transfection, and an additional transfection was carried out 24 h after the first (double transfection). Experiments were performed 72 h after the first siRNA transfection. Knockdown efficiency was confirmed by protein blot.

Lentivirus production. Human UVSSA cDNA was cloned in frame with sequences encoding a C-terminal V5 tag into pLenti6/V5-D-TOPO (Invitrogen) to generate plenti6/UVSSA-V5. Sequences encoding the truncation and amino-acid substitution mutants were generated from plenti6/UVSSA-V5 by site-directed PCR mutagenesis using specific primer sets (primer sequences are available from T.O. upon request), PrimeSTAR HS high-fidelity DNA polymerase (TaKaRa) and the DpnI restriction enzyme (NEB). For lentivirus production, HEK293FT cells were transfected with UVSSA-encoding plasmids together with ViraPower Packaging Mix (Invitrogen) containing pLP1, pLP2 and pLP/VSVG using Lipofectamine 2000 (Invitrogen). Viral particles were collected 48 h after transfection and concentrated using PEG-it Virus Precipitation Solution (System Biosciences).

Cell lines and culture. The following cell lines were used for this study: 48BR and 1BR (normal human primary fibroblasts); Kps2, Kps3, XP24KO and UV^SS24TA (primary fibroblasts from individuals with UV^SS-A); XP70TO (primary fibroblast from a mild case of xeroderma pigmentosum); CS2AW (primary fibroblast from individuals with CS-A); CS10LO (primary fibroblasts from individuals with CS-B); XP15BR (primary fibroblasts from individuals with xeroderma pigmentosum-A); and HEK293T and HEK293FT (human embryonic kidney lines). All cells were maintained in DMEM (WAKO) supplemented with 10% FCS (Hyclone) and antibiotics, unless otherwise noted.

33. Li, H. & Durbin, R. Fast and accurate short read alignment with Burrows-Wheeler transform. *Bioinformatics* **25**, 1754–1760 (2009).
34. DePristo, M.A. *et al.* A framework for variation discovery and genotyping using next-generation DNA sequencing data. *Nat. Genet.* **43**, 491–498 (2011).
35. McKenna, A. *et al.* The Genome Analysis Toolkit: a MapReduce framework for analyzing next-generation DNA sequencing data. *Genome Res.* **20**, 1297–1303 (2010).
36. Albers, C.A. *et al.* Dindel: accurate indel calls from short-read data. *Genome Res.* **21**, 961–973 (2011).
37. Wang, K., Li, M. & Hakonarson, H. ANNOVAR: functional annotation of genetic variants from high-throughput sequencing data. *Nucleic Acids Res.* **38**, e164 (2010).
38. Ng, P.C. & Henikoff, S. SIFT: predicting amino acid changes that affect protein function. *Nucleic Acids Res.* **31**, 3812–3814 (2003).



Mutations affecting components of the SWI/SNF complex cause Coffin-Siris syndrome

Yoshinori Tsurusaki¹, Nobuhiko Okamoto², Hirofumi Ohashi³, Tomoki Kosho⁴, Yoko Imai⁵, Yumiko Hibi-Ko⁵, Tadashi Kaname⁶, Kenji Naritomi⁶, Hiroshi Kawame^{7,8}, Keiko Wakui⁴, Yoshimitsu Fukushima⁴, Tomomi Homma⁹, Mitsuihiro Kato¹⁰, Yoko Hiraki¹¹, Takanori Yamagata¹², Shoji Yano¹³, Seiji Mizuno¹⁴, Satoru Sakazume¹⁵, Takuma Ishii^{15,16}, Toshiro Nagai¹⁵, Masaaki Shiina¹⁷, Kazuhiro Ogata¹⁷, Tohru Ohta¹⁸, Norio Niikawa¹⁸, Satoko Miyatake¹, Ippeï Okada¹, Takeshi Mizuguchi¹, Hiroshi Doi¹, Hirotomo Saitsu¹, Noriko Miyake¹ & Naomichi Matsumoto¹

By exome sequencing, we found *de novo* SMARCB1 mutations in two of five individuals with typical Coffin-Siris syndrome (CSS), a rare autosomal dominant anomaly syndrome. As SMARCB1 encodes a subunit of the SWI/SNF complex, we screened 15 other genes encoding subunits of this complex in 23 individuals with CSS. Twenty affected individuals (87%) each had a germline mutation in one of six SWI/SNF subunit genes, including SMARCB1, SMARCA4, SMARCA2, SMARCE1, ARID1A and ARID1B.

Chromatin remodeling factors regulate the gene accessibility and expression by dynamic alteration of chromatin structure. SWI/SNF complexes have important roles in lineage specification, maintenance of stem cell pluripotency and tumorigenesis^{1–5}. These complexes are composed of evolutionarily conserved core subunits and variant subunits. Brahma-associated factor (BAF) and Polybromo BAF (PBAF) complexes constitute two major subclasses^{1–5}. It has been suggested that the BAF complex is similar to the yeast SWI/SNF complex and that the PBAF complex is more like the chromatin remodelling complex (RSC) in yeast, which is required for cell cycle progression through mitosis⁶. However, several subunits that are common

to both BAF and PBAF complexes are predicted to be related to the regulation of lineage- and tissue-specific gene expression².

Coffin-Siris syndrome (MIM 135900) is a rare congenital anomaly syndrome characterized by growth deficiency, intellectual disability, microcephaly, coarse facial features and hypoplastic nail of the fifth finger and/or toe (Fig. 1 and Supplementary Table 1)⁷. The majority of affected individuals represent sporadic cases, which is compatible with an autosomal dominant inheritance mechanism. The genetic cause for this syndrome has not been elucidated.

To identify the genetic basis of CSS, we performed whole-exome sequencing of five typical affected individuals (Supplementary Methods). Taking into account our model that assumes that an abnormality in a causal gene would be shared in two or more subjects, 51 variants were identified as candidates (Supplementary Table 2). All the variants were also examined by Sanger sequencing of PCR products amplified using genomic DNA from the five affected individuals and their parents. Nine variants were found to be false positives, 40 were inherited from either the father or mother, and 2 *de novo* heterozygous mutations of *SMARCB1* were found in 2 affected individuals (c.1130G>A (p.Arg377His) and c.1091_1093del AGA (p.Lys364del)) (Table 1, Supplementary Fig. 1 and Supplementary Methods). Two *de novo* coding-sequence mutations occurring within a specific gene is an extremely unlikely event⁸, supporting the idea that *SMARCB1* is a causative gene in CSS. Next, we screened *SMARCB1* in 23 individuals with CSS by high-resolution melting analysis⁹ and identified the mutation encoding the p.Lys364del alteration in two additional individuals, including one of Arab descent (subject 22) (Table 1 and Supplementary Fig. 1). As the mutation detection rate was relatively low (4 of 23, only 17.4%), we screened 15 additional genes encoding other SWI/SNF subunits (Supplementary Table 3). Unexpectedly, four other subunits, *SMARCA4* (also known as *BRG1*), *SMARCE1*, *ARID1A* and *ARID1B* were also found to be mutated (Table 1 and Supplementary Figs. 2–5). In subject 10, a c.2144C>T mutation in *ARID1B* (encoding p.Pro715Leu) was found in addition to the c.5632delG mutation in *ARID1B*. RT-PCR products that were amplified from total RNA from this subject's lymphoblastoid cells were cloned into the pCR4-TOPO vector. The two mutations were present on different alleles, according to sequencing of clones containing each allele (data not shown). As the c.5632delG mutation is

¹Department of Human Genetics, Yokohama City University Graduate School of Medicine, Yokohama, Japan. ²Division of Medical Genetics, Osaka Medical Center and Research Institute for Maternal and Child Health, Izumi, Japan. ³Division of Medical Genetics, Saitama Children's Medical Center, Iwatsuki, Japan. ⁴Department of Medical Genetics, Shinshu University School of Medicine, Matsumoto, Japan. ⁵Division of Pediatrics, Japanese Red Cross Medical Center, Tokyo, Japan. ⁶Department of Medical Genetics, University of the Ryukyus Faculty of Medicine, Okinawa, Japan. ⁷Department of Genetic Counseling, Graduate School of Humanities and Sciences, Ochanomizu University, Tokyo, Japan. ⁸Division of Medical Genetics, Nagano Children's Hospital, Azumino, Japan. ⁹Division of Pediatrics, Yamagata Prefectural and Sakata Municipal Hospital Organization, Nihonkai General Hospital, Sakata, Japan. ¹⁰Department of Pediatrics, Yamagata University Faculty of Medicine, Yamagata, Japan. ¹¹Hiroshima Municipal Center for Child Health and Development, Hiroshima, Japan. ¹²Department of Pediatrics, Jichi Medical University, Tochigi, Japan. ¹³Genetics Division, Department of Pediatrics, Los Angeles County and University of Southern California Medical Center, Keck School of Medicine, University of Southern California, Los Angeles, California, USA. ¹⁴Department of Pediatrics, Central Hospital, Aichi Human Service Center, Kasugai, Japan. ¹⁵Department of Pediatrics, Koshigaya Hospital, Dokkyo University School of Medicine, Koshigaya, Japan. ¹⁶Nakagawa-No-Sato, Hospital for the Disabled, Saitama, Japan. ¹⁷Department of Biochemistry, Yokohama City University Graduate School of Medicine, Yokohama, Japan. ¹⁸Research Institute of Personalized Health Sciences, Health Sciences University of Hokkaido, Ishikari-Tobetsu, Japan. Correspondence should be addressed to N. Matsumoto (naomat@yokohama-cu.ac.jp) or N. Miyake (nmiyake@yokohama-cu.ac.jp).

Received 29 September 2011; accepted 10 February 2012; published online 18 March 2012; doi:10.1038/ng.2219



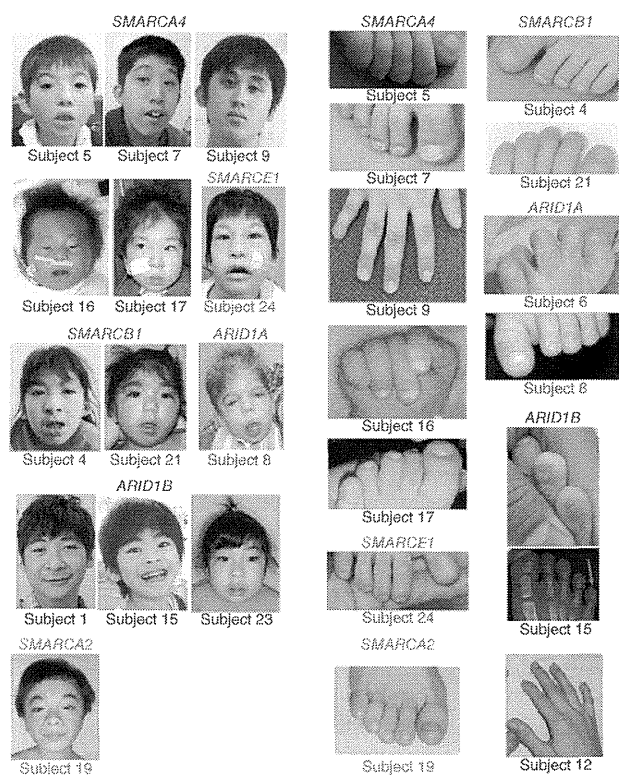


Figure 1 Photographs of individuals with Coffin-Siris syndrome. The faces (left) and hypoplastic-to-absent nail of the fifth finger or toe (right) of affected individuals are shown with the color-coded names of the corresponding mutated genes. The green arrow indicates the absence of the distal phalanx in the fifth toe. No obvious hypoplastic nails were observed in subjects 12 or 19. Consent for all the photographs was obtained from the families of the affected individuals.

in mice¹⁰. However, in humans, abnormalities in both *SMARCA4* and *SMARCA2* are found in CSS, indicating that the in-frame partial deletion of the gene encoding BRM in subject 19 has a specific mutational effect different from that of simple inactivation in mice. These data support the idea that abnormalities in the BRG1-BAF and BRM-BAF complexes can cause the abnormal neurological development in CSS.

All the mutated genes found in CSS, except for *SMARCE1*, have been reported to be associated with tumorigenesis^{1,2}. Among the 23 subjects with CSS, only subject 3 with an *ARID1A* mutation presented with hepatoblastoma. To our knowledge, haploinsufficiency and/or homozygous inactivation of *ARID1A* have been found in several types of cancer but not in hepatoblastoma. Malignancies were not detected in any of the other subjects with CSS examined here. It remains to be seen whether malignancies are robustly associated with CSS.

Given the fact that all the mutations in *ARID1A* and *ARID1B* in CSS were predicted to cause protein truncation, we proposed that haploinsufficiency of these two genes must be able to cause CSS. cDNA analysis of lymphoblastoid cell lines from subjects 1, 6 and 23 indicated that the mutated transcripts were subject to nonsense-mediated mRNA decay (Supplementary Fig. 8). In subject 10, the *ARID1B* mutation associated with the creation of a premature stop codon in the last exon did not result in nonsense-mediated mRNA decay as expected (Supplementary Fig. 8).

In regard to the other mutated genes, germline heterozygous truncation mutations in *SMARCB1* and *SMARCA4* have been reported

very likely to be deleterious (as it results in a truncated protein), the c.2144C>T mutation is likely to be a rare polymorphism. Of note, subject 12, who presented an atypical facial appearance and indistinct hypoplastic nails, had two interstitial deletions at 6q25.3–q27 involving *ARID1B*, as detected by a SNP array (Supplementary Fig. 6 and Supplementary Methods). Furthermore, subject 14 was found to have an interstitial deletion of *SMARCA2* by a SNP array (Supplementary Fig. 7 and Supplementary Methods). No other copy-number changes involving genes encoding SWI/SNF complex components were found in subjects 2, 14 or 18 by array analysis. The overall mutation detection rate was 87%. In total, 20 of the 23 subjects had a mutation affecting one of the six SWI/SNF subunits.

Mutations in CSS were identified in the BAF-specific subunits *ARID1A* and *ARID1B* but not in PBAF-specific subunits (*BRD7*, *ARID2* and *PBRM1*) (Supplementary Table 3). In addition, mutations were identified in *SMARCA4* (*BRG1*) as well as in *SMARCA2* (*BRM*) (Supplementary Table 3). The BRG1 and BRM proteins are mutually exclusive catalytic ATP subunits in mammalian SWI/SNF complexes. Of note, the majority of heterozygous *Smarca4*-null mice survive with susceptibility to neoplasia, with a minority dying after birth because of exencephaly, whereas homozygous *Smarca2*-null mice are viable and fertile⁴. In *Smarca2*-null mice, Brg1 is upregulated, suggesting that Brg1 can functionally replace Brm

Table 1 Mutations in individuals with Coffin-Siris syndrome

Subject ID	Gene	Mutation	Alteration	Type	Control allele frequency ^a
4	<i>SMARCB1</i>	c.1091_1093del	AGA p.Lys364del	<i>De novo</i>	0/502
11	<i>SMARCB1</i>	c.1130G>A	p.Arg377His	<i>De novo</i>	0/500
21	<i>SMARCB1</i>	c.1091_1093del	AGA p.Lys364del	NC	0/502
22	<i>SMARCB1</i>	c.1091_1093del	AGA p.Lys364del	NC	0/502
9	<i>SMARCA4</i>	c.1636_1638del	AAG p.Lys546del	<i>De novo</i>	0/350
7	<i>SMARCA4</i>	c.2576C>T	p.Thr859Met	<i>De novo</i>	0/368
5	<i>SMARCA4</i>	c.2653C>T	p.Arg885Cys	<i>De novo</i>	0/368
16	<i>SMARCA4</i>	c.2761C>T	p.Leu921Phe	<i>De novo</i>	0/368
25	<i>SMARCA4</i>	c.3032T>C	p.Met1011Thr	NC	0/372
17	<i>SMARCA4</i>	c.3469C>G	p.Arg1157Gly	<i>De novo</i>	0/368
19	<i>SMARCA2</i>	Partial deletion		<i>De novo</i>	–
24	<i>SMARCE1</i>	c.218A>G	p.Tyr73Cys	<i>De novo</i>	0/368
3	<i>ARID1A</i>	c.31_56del	p.Ser11Alafs*91	NC	0/330
6	<i>ARID1A</i>	c.2758C>T	p.Gln920*	NC	0/376
8	<i>ARID1A</i>	c.4003C>T	p.Arg1335*	<i>De novo</i>	–
1	<i>ARID1B</i>	c.1678_1688del	p.Ile560Glyfs*89	<i>De novo</i>	–
15	<i>ARID1B</i>	c.1903C>T	p.Gln635*	<i>De novo</i>	–
23	<i>ARID1B</i>	c.3304C>T	p.Arg1102*	<i>De novo</i>	–
10	<i>ARID1B</i>	c.2144C>T	p.Pro715Leu	NC	0/368
10	<i>ARID1B</i>	c.5632del	G p.Asp1878Metfs*96	NC	0/374
12	<i>ARID1B</i>	Microdeletion		NC	–

NC, not confirmed because parental samples were unavailable.

^aThe numbers indicate the observed allele frequency (alleles harboring the change/total tested alleles) in Japanese controls. None of the mutations was found in dbSNP132, the 1000 Genomes database or the National Heart, Lung, and Blood Institute (NHLBI) GO exome sequencing project database. –, not tested.

in individuals with rhabdoid tumor predisposition syndromes 1 (RTPS1; MIM 609322) and 2 (RTPS2; MIM 613325)^{11,12}, and various types of *SMARCB1* mutations (missense, in-frame deletion, nonsense and splice site) have been found in the germline of individuals with familial and sporadic schwannomatosis (MIM 162091)^{13,14}. Furthermore, mice with heterozygous knockout of *Smarca4* or *Smarcb1* were prone to tumor development². All the mutations in *SMARCA4* and *SMARCB1* in individuals with CSS were non-truncating (either missense or in-frame deletions), implying that they exert gain-of-function or dominant-negative effects (excluding haploinsufficiency as a cause). It is noteworthy that comparable germline mutations in *SMARCB1* have such different phenotypic consequences in their association with the phenotypes of CSS and schwannomatosis. The *SMARCB1* mutations in CSS and those in schwannomatosis are indeed different according to the Human Gene Mutation Database. With regard to the *SMARCA2* interstitial deletion in CSS, the change maintained the coding sequence reading frame but removed exons 20–27 that encode the HELICc domain. RT-PCR analysis confirmed the deletion of exons 20–27 at the cDNA level (Supplementary Fig. 7). These data suggest the importance of the HELICc domain in the *SMARCA2* protein.

The various types of mutations in the genes encoding different SWI/SNF components resulted in similar CSS phenotypes. This suggests that the SWI/SNF complexes coordinately regulate chromatin structure and gene expression. This is the first report, to our knowledge, of germline mutations in SWI/SNF complex genes associated with a multiple congenital anomaly syndrome, highlighting new biological aspects of SWI/SNF complexes in humans. Similarly, genes encoding SNF2-related proteins, which are implicated as chromatin remodeling factors outside of SWI/SNF complexes, are mutated in different syndromes, including in α -thalassaemia/mental retardation syndrome X-linked (*ATRX*; *ATRX* mutations) and in coloboma, heart defect, atresia choanae, retarded growth and development, genital abnormality and ear abnormality (*CHARGE* syndrome (*CHD7* haploinsufficiency)³. We expect that more mutations affecting chromatin remodeling factors will be found in different human diseases.

URLs. Human Gene Mutation Database, <https://portal.biobase-international.com/cgi-bin/portal/login.cgi>.

Note: Supplementary information is available on the Nature Genetics website.

ACKNOWLEDGMENTS

We thank all the family members for participating in this study. This work was supported by research grants from the Ministry of Health, Labour and Welfare (to N. Miyake, H.S. and N. Matsumoto), the Japan Science and Technology Agency (to N. Matsumoto), the Strategic Research Program for Brain Sciences (to N. Matsumoto), the Japan Epilepsy Research Foundation (to H.S.) and the Takeda Science Foundation (to N. Matsumoto and N. Miyake). This study was also funded by a Grant-in-Aid for Scientific Research on Innovative Areas (Foundation of Synapse and Neurocircuit Pathology) from the Ministry of Education, Culture, Sports, Science and Technology of Japan (to N. Matsumoto), a Grant-in-Aid for Scientific Research from the Japan Society for the Promotion of Science (to N. Matsumoto), a Grant-in-Aid for Young Scientists from the Japan Society for the Promotion of Science (to N. Miyake and H.S.) and a Grant for 2011 Strategic Research Promotion of Yokohama City University (to N. Matsumoto). This study was performed at the Advanced Medical Research Center at Yokohama City University. Informed consent was obtained from all the families of affected individuals. The Institutional Review Board of Yokohama City University approved this study.

AUTHOR CONTRIBUTIONS

Y.T., S. Miyatake, I.O., H.D., H.S. and N. Miyake performed exome sequencing and Sanger sequencing. Y.T., M.S., K.O., I.O., T.M., H.D., H.S. and N. Miyake performed data management and analysis. N.O., H.O., T. Koshio, Y.I., Y.H.-K., T. Kaname, K.N., H.K., K.W., Y.F., T.H., M.K., Y.H., T.Y., S.Y., S. Mizuno, S.S., T.I., T.N., T.O. and N.N. provided clinical materials after careful evaluation. Y.T., N. Miyake and N. Matsumoto wrote the manuscript. N. Matsumoto designed and oversaw all aspects of the study.

COMPETING FINANCIAL INTERESTS

The authors declare no competing financial interests.

Published online at <http://www.nature.com/naturegenetics/>.

Reprints and permissions information is available online at <http://www.nature.com/reprints/index.html>.

1. Reisman, D., Glaros, S. & Thompson, E.A. *Oncogene* **28**, 1653–1668 (2009).
2. Wilson, B.G. & Roberts, C.W. *Nat. Rev. Cancer* **11**, 481–492 (2011).
3. Clapier, C.R. & Cairns, B.R. *Annu. Rev. Biochem.* **78**, 273–304 (2009).
4. Bultman, S. *et al. Mol. Cell* **6**, 1287–1295 (2000).
5. Hargreaves, D.C. & Crabtree, G.R. *Cell Res.* **21**, 396–420 (2011).
6. Xue, Y. *et al. Proc. Natl. Acad. Sci. USA* **97**, 13015–13020 (2000).
7. Coffin, G.S. & Siris, E. *Am. J. Dis. Child.* **119**, 433–439 (1970).
8. Bamshad, M.J. *et al. Nat. Rev. Genet.* **12**, 745–755 (2011).
9. Wittwer, C.T., Reed, G.H., Gundry, C.N., Vandersteen, J.G. & Pryor, R.J. *Clin. Chem.* **49**, 853–860 (2003).
10. Reyes, J.C. *et al. EMBO J.* **17**, 6979–6991 (1998).
11. Schneppenheim, R. *et al. Am. J. Hum. Genet.* **86**, 279–284 (2010).
12. Taylor, M.D. *et al. Am. J. Hum. Genet.* **66**, 1403–1406 (2000).
13. Boyd, C. *et al. Clin. Genet.* **74**, 358–366 (2008).
14. Hadfield, K.D. *et al. J. Med. Genet.* **45**, 332–339 (2008).



